Available online at www.sciencedirect.com
SCIENCE DIRECT®
International Journal of Multiphase Flow 30 (2004) 521–550
International Journal of Multiphase Flow
www.elsevier.com/locate/ijmulflow

A theoretical model for gas–liquid slug flow in down inclined ducts

A. Dyment *, A. Boudlal

Laboratoire de Mécanique de Lille, UMR CNRS 8107, Université des Sciences et Technologies de Lille, Bâtiment M3 – Mécanique, 59655 Villeneuve d'Ascq Cedex, France

Received 1 April 2003; received in revised form 4 February 2004

Abstract

Analytical solutions are obtained for flows in downwardly inclined ducts, partly filled by a liquid and containing finite amplitude moving jumps. A unified theory for both roll waves and periodic slug flows in rounded ducts of arbitrary cross-section is worked out by means of some simplifications. The article is focused on slugs: a set of equations is obtained, which predicts the transition between roll waves and slug regimes and gives access to all flow characteristics without any need of closure laws concerning either the speed of propagation or the slug length. As a result, we gain a new insight on the physical structure of slug flow. The proposed model is valid for sufficient inclination, small pressure gradient along the duct and negligible superficial tension. Owing to assumptions, only main trends and orders of magnitude observed in experiments are to be checked. In this connection the model fits most of the previously published experimental results obtained in ducts of circular cross-section: the domain of occurrence of downwardly propagating slugs is satisfactorily predicted, the limitations in drift velocity and in liquid layer thickness are demonstrated and upwardly propagating slugs are possible.
© 2004 Elsevier Ltd. All rights reserved.

Keywords: Inclined ducts; Gas–liquid flow; Periodic slugs

1. Introduction

1.1. Roll waves and slug flow

Two phase gas–liquid flows in nearly horizontal ducts are of considerable interest in industry processes and equipments. Over a range of flow rates two complex regimes are met, namely roll

* Corresponding author. Tel.: +33-3-20-43-42-49; fax: +33-3-20-33-70-88.
E-mail address: arthur.dyment@univ-lille1.fr (A. Dyment).

0301-9322/$ - see front matter © 2004 Elsevier Ltd. All rights reserved.
doi:10.1016/j.ijmultiphaseflow.2004.02.002

waves and slugs, which have some common features for they exhibit a periodic structure moving with a constant velocity. Roll waves consist of a periodic pattern of bores separated by continuous profiles of the interface, whereas slugs present successive cells made of liquid plugs which are separated from one another by a liquid layer topped by a gaseous bubble.

During the three last decades of the 20th century, investigation of slug flow, principally instigated by petroleum industry needs, has been intensive. One of the main reasons for carrying out research in this domain is the generation of vibrations induced by slugs, which may be followed by destructive damage in case of resonance.

The relation between flow conditions and slug occurrence has been modelled on the bases of continuous one-dimensional conservative laws for each phase (Dukler and Hubbard, 1975; Taitel and Dukler, 1976; Taitel and Barnea, 1990). Supplementary laws expressing empirical correlations about the wall to fluid and the interface interactions are necessary in order to operate with a full set of equations, able to provide velocities, pressure drops and characteristic lengths if the liquid and gas fluxes are known.

The first aim of scientists has been to draw up maps of flow patterns in terms of liquid and gas input rates (Barnea et al., 1980; Barnea and Taitel, 1986) essentially by visual observation, and later with the help of void fraction detection and pressure fluctuation measurements.

The sudden increase in both the liquid level and the pressure observed at the passage of a slug has raised the occurrence of associated abrupt jumps (Fan et al., 1993). Our first purpose in the present article will be to take this characteristic into account when working out the new model.

The transition from smooth stratified flow to complex regimes is usually tackled by resorting to stability theory (Lin and Hanratty, 1986; Boudlal and Dyment, 1996; among others). When it is perturbated, a steady flow becomes unstable if certain criteria are satisfied and it evolves towards wave breaking, which gives rise to roll waves. Attempts have been made in order to understand this unsteady nonlinear process for a liquid flowing in board open slightly inclined channels (Kranenburg, 1992; Yu and Kevorkian, 1992) and for a two layer system (Liapidevskii, 2000). Roll waves themselves may be unstable and slugging may be initiated by waves growing in amplitude, steepening and coalescing, with their crests touching the top of the conduit (Woods et al., 2000).

1.2. The frame of the present model

The gas–liquid flows considered herein are simple ones in order for the analytical approach to go as far as possible. They take place in down sloping cylindrical ducts.

The liquid flows subject to gravity and friction forces acting on the wall. The interfacial friction and the gas friction at the wall are neglected and the gas pressure is considered as almost constant, which implies that the gas momentum rate is small enough with respect to the liquid one. (Nevertheless, nothing is prescribed by this assumption concerning the flow rates.) Due to the contrast in density, previous events are encountered when the velocities of both liquid and gas are of the same order of magnitude. (The most elementary configuration corresponds to no forced input of gas, which is only swept along by the running liquid.) These circumstances require the gas input be not too high and the duct be down sloping with a sufficient inclination, as the gravity is the single force able to carry off the liquid downwardly. However, at the same time, the slope β is supposed enough gentle to meet $\sin\beta \simeq \beta$, $\cos\beta \simeq 1$.

Further assumptions are made. No dispersed gaseous bubbles are contained in the liquid. The superficial tension is not taken into account, which requires the transverse dimension of the conduit to be large enough. As a consequence, the Reynolds number is large too, so the resistance at the wall can be expressed by standard turbulence laws involving the hydraulic diameter. In this case, it is known that the streamwise velocity profile is not far from uniform. Thanks to all the aforementioned simplifications, as long as slugs do not occur, the same formulation will be obtained as for a liquid flowing alone, beneath a gas at constant pressure.

Two parameters, directly connected to the cross-section shape will play an important part, $D = \frac{d^2(a^{-2})}{dh^2}$ and $E = \frac{d\delta}{dh}$ where h is the liquid level, a the wetted section and δ the hydraulic diameter, $\delta = \frac{4a}{k}$, k being the wetted perimeter. For all round shaped ducts D is positive whatever h may be (Dyment, 1998). As for E, it turns out that for closed conduits E is necessarily negative past a certain degree of filling, namely for $\tilde{h} < h < H$, H being the height of the duct section. A linear stability analysis shows that the flow is unconditionally stable for $h = \tilde{h}$ and the more unstable the farther h is from $\tilde{h}$.

Instability gives rise to roll waves with discontinuities, which necessarily represent rising jumps since D is positive, a result still standing for choked discontinuities, so called because downstream the duct is entirely filled by the liquid (Dyment, 1998). The passage from roll waves to slugs consists of piecing together the continuous interface profiles with liquid stubs, one end of which is matched to the neighbouring liquid layer through a choked bore.

The nature of all periodic waves containing bores is connected to the sign of the critical value E^*. For $E^* > 0$, downwardly propagating roll waves and slugs are obtained, similarly to the roll waves solution in open channels. When $E^* < 0$, i.e. $\tilde{h} < h < H$, waves moving upward with regard to the flowing liquid are predicted.

Previous results are plotted in a two-dimensional universal regime map providing the ranges of possible roll waves and periodic slugs according to their nature, solely in terms of the critical height and the critical friction factor to slope ratio.

A more usual representation of slugs, with superficial velocities of both liquid and gas, is introduced. Comparison with available experimental results in circular ducts indicates that the proposed model is relevant.

2. Geometrical properties of ducts

As the flow in a cylindrical duct which is partly filled by a liquid depends on the cross-section shape, some geometrical properties of the conduit must be pointed out.

The cross-section is supposed round, smoothly shaped and symmetrical about the longitudinal vertical plane containing the duct axis. The duct is downwardly inclined with an angle β. The frame of reference is chosen as follows: the Ox axis is parallel to the direction of the duct with the origin O at the bottom; Oz is contained in the vertical plane and Oy completes the system of coordinates. Let $y = \eta(z)$ define the half of the duct corresponding to $y > 0$ (Fig. 1). $z = h$ represents the free surface which is independent of y in the frame of the shallow water theory. We introduce $b = \eta(h)$, $a = \int_0^h \eta \, dz$, $k = \int_0^h [1 + (\frac{d\eta}{dz})^2]^{1/2} dz$, $f = \frac{1}{a}$ and φ by $d\varphi = a\,dh$ with $\varphi(0) = 0$. The hydraulic diameter is $\delta = \frac{4a}{k}$ and $c = (\frac{ga}{b})^{1/2}$ is the wave speed of small disturbances, g being the gravitational acceleration. Obviously $\frac{da}{dh} = b$, $\frac{d\varphi}{dh} = a$, $c^2 = g\frac{d\varphi}{da}$, so that

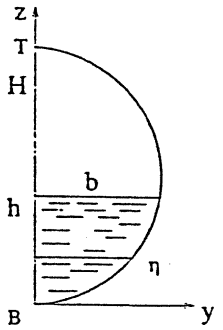

Fig. 1. Half cross-section of the conduit.

$$a^2c^2 = -g\frac{\mathrm{d}\varphi}{\mathrm{d}f}. \tag{1}$$

Function f is a decreasing one of φ with $\frac{\mathrm{d}f}{\mathrm{d}\varphi} = -\infty$ at the bottom and $\frac{\mathrm{d}f}{\mathrm{d}\varphi} = 0$ at the top where $h = H$, $a = A$, $k = K$, $\delta = \Delta = \frac{4A}{K}$, $\varphi = \phi$, $c \to \infty$ and $f = F = \frac{1}{A}$.

An important parameter is the fundamental derivative D (Dyment, 1981, 1998):

$$D = \frac{\mathrm{d}^2(a^{-2})}{\mathrm{d}h^2} = -2g\frac{\mathrm{d}(a^{-2}c^{-2})}{\mathrm{d}h} = \frac{2}{f}\frac{\mathrm{d}^2f}{\mathrm{d}\varphi^2}. \tag{2}$$

For a round smoothly shaped duct, $\frac{\mathrm{d}^2b}{\mathrm{d}h^2}$ is negative, yielding D positive whatever h. Then, it results from (1) and (2) that f is a decreasing convex function of φ.

The second important parameter is

$$E = \frac{\mathrm{d}\delta}{\mathrm{d}h} = \frac{4}{k^2}\left(kb - a\left[1 + \left(\frac{\mathrm{d}b}{\mathrm{d}h}\right)^2\right]^{1/2}\right). \tag{3}$$

It may be shown (Appendix A) that δ is a concave function of h with $\delta = 0$ at $h = 0$, $E \to \infty$ at $h = H$ and a maximum at a value of h termed $\tilde{h}$. As a result, except H there is another height h_Δ for which δ is equal to Δ. When h is higher than h_Δ, a second height, termed h_δ, exists, providing the same value of δ: the height h_δ is a decreasing function of h.

As the cross-section is round, its bottom can be locally represented by the osculating parabola $\eta = (2R_\mathrm{B}z)^{1/2}$, R_B being the radius of curvature at the bottom B. In the vicinity of B we have $b^2 \simeq 2R_\mathrm{B}h$, $\frac{\mathrm{d}b}{\mathrm{d}h} \simeq \frac{R_\mathrm{B}}{b}$, $a \simeq \frac{b^3}{3R_\mathrm{B}}$, $k \simeq b + \frac{b^3}{6R_\mathrm{B}^2}$, $\varphi \simeq \frac{b^5}{15R_\mathrm{B}^2}$, $c \simeq (\frac{2gh}{3})^{1/2}$, $\delta \simeq \frac{8h}{3}$, $E \simeq \frac{8}{3}$ and $D \simeq \frac{27}{2R_\mathrm{B}h^5}$.

At the top T, where the radius of curvature is R_T, we have similarly:

$$\eta \simeq [2R_\mathrm{T}(H-z)]^{1/2}, \quad b^2 \simeq 2R_\mathrm{T}(H-h), \quad \frac{\mathrm{d}b}{\mathrm{d}h} \simeq -\frac{R_\mathrm{T}}{b}, \quad a \simeq A - \frac{b^3}{3R_\mathrm{T}},$$

$$k \simeq K - b - \frac{b^3}{6R_\mathrm{T}^2}, \quad \varphi \simeq \phi - A(H-h), \quad c \simeq \left(\frac{gA}{b}\right)^{1/2}, \quad \delta \simeq \Delta\left(1 + \frac{b}{K}\right),$$

$$E \simeq -\frac{\Delta R_\mathrm{T}}{Kb} \quad \text{and} \quad D \simeq \frac{2R_\mathrm{T}}{A^3b}.$$

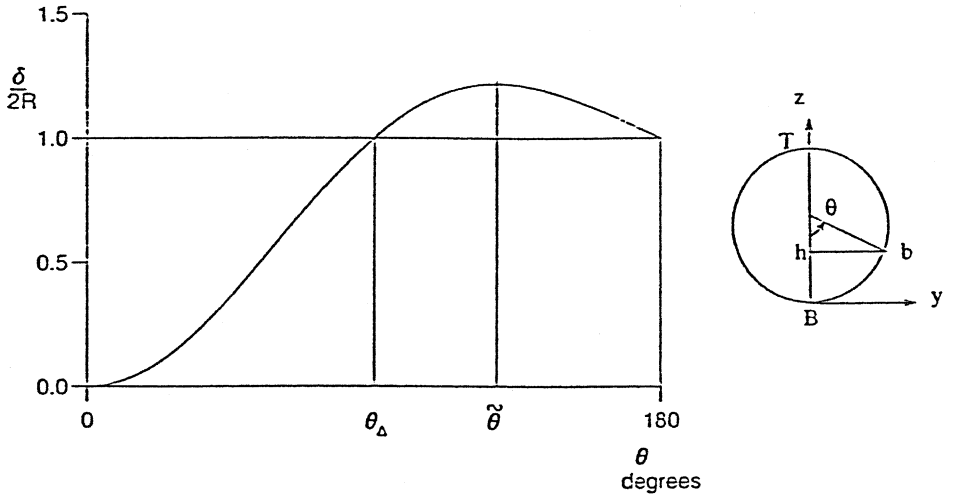

Fig. 2. The hydraulic diameter for circular ducts, $\tilde{\theta} = 128.7°$, $\theta_{\Delta} = 90°$.

Consider the important example of a circular cross-section of radius R. With the angle θ defined in Fig. 2, we have:

$$h = R(1-\cos\theta), \quad b = R\sin\theta, \quad a = \frac{R^2}{4}(2\theta - \sin 2\theta), \quad k = R\theta,$$

$$c^2 = \frac{gR}{4}\frac{(2\theta-\sin 2\theta)}{\sin\theta}, \quad \delta = R\frac{(2\theta-\sin 2\theta)}{\theta}, \quad \frac{2g\delta}{c^2} = \frac{8\sin\theta}{\theta},$$

$$\varphi = \frac{R^3}{2}\left(\sin\theta - \frac{\sin^3\theta}{3} - \theta\cos\theta\right), \quad D = \frac{256(1+5\sin^2\theta-\theta\cot\theta)}{R^6(2\theta-\sin 2\theta)^4} \quad \text{and}$$

$$E = \frac{\sin 2\theta - 2\theta\cos 2\theta}{\theta^2\sin\theta}.$$

The hydraulic diameter is plotted in Fig. 2. The maximum of δ occurs for $\tilde{\theta} \simeq 128.73°$ yielding $\frac{\tilde{h}}{2R} \simeq 0.813$ and $\frac{\tilde{\delta}}{2R} \simeq 1.23$. The corresponding values of f and φ are $\tilde{f} = 1.149F$, $\tilde{\varphi} = 0.645\phi$, with $F = \frac{2}{\pi R^2}$ and $\phi = \frac{\pi R^3}{2}$.

3. Criteria of stability

3.1. Linear stability analysis

Taking into account all aforementioned assumptions in Section 1.2, the governing equations expressing the conservation of mass and momentum are:

$$\frac{\partial a}{\partial t} + \frac{\partial}{\partial x}(au) = 0, \tag{4}$$

$$\frac{\partial u}{\partial t} + u\frac{\partial u}{\partial x} + g\frac{\partial h}{\partial x} = g\beta - \frac{\psi u^2}{2\delta}. \tag{5}$$

In previous equations t is the time and ψ the friction coefficient at the wall. The second equation is obtained with the help of the hydrostatic distribution of pressure $\rho g(h-z)$, ρ being the liquid density, and the origin of pressure being chosen in the gas which tops the liquid. The gas velocity v is deduced from a and u with the help of the conservation of mass for both fluids, which expresses that $au + (A-a)v$ is constant.

The friction factor ψ is assumed to be

$$\psi = \gamma u^{-m}\delta^{-n}, \tag{6}$$

where γ, m and n are constant, with $0 \leqslant m < 1$ and $0 \leqslant n < 1$ too. For smooth turbulent flows, $m = n$ and $\gamma = \kappa \nu^m$, κ being a constant and ν the kinematic viscosity. In practice, $m = 0.2$ and $\kappa = 0.184$. For rough turbulent flows, $m = 0$, and $n = 0$ or $n = \frac{1}{3}$. The last case corresponds to Manning's law when $\gamma = 0.3\varepsilon^{1/3}$, ε being the mean height of the roughness. As the liquid and gas velocities are supposed to be of the same order of magnitude, the interfacial shear stress is negligible because it is proportional to the gas density (Taitel and Barnea, 1990).

To sum up, the pressure gradient and interfacial friction effects are neglected with regard to wall friction and gravity effects, which implies that the duct inclination is not too small.

We consider a uniform flow (subscript 0). According to (5), u_0 and h_0 are connected by

$$\psi_0 u_0^2 = 2g\beta\delta_0. \tag{7}$$

The resistance law (6) can be written

$$\frac{\psi}{\psi_0} = \left(\frac{u_0}{u}\right)^m \left(\frac{\delta_0}{\delta}\right)^n. \tag{8}$$

Now, a small disturbance is superimposed: $h = h_0 + h'$, $u = u_0 + u'$.

The linearization of Eqs. (4) and (5), a rearrangement made with the help of (6) and (7) and the elimination of u' lead to

$$\frac{u_0}{(2-m)g\beta}\left[\frac{\partial}{\partial t} + (u_0 - c_0)\frac{\partial}{\partial x}\right]\left[\frac{\partial}{\partial t} + (u_0 + c_0)\frac{\partial}{\partial x}\right](h') + \left[\frac{\partial}{\partial t} + u_0\left(1 + \frac{1+n}{2-m}\frac{c_0^2 E_0}{g\delta_0}\right)\frac{\partial}{\partial x}\right](h') = 0.$$

Making use of the method promoted by Whitham (1974), the conditions for stability tie the three speeds of propagation brought to evidence in this equation: $u_0 - c_0 < u_0\left[1 + \frac{1+n}{2-m}\frac{c_0^2 E_0}{g\delta_0}\right] < u_0 + c_0$. Conversely, taking (7) into account, the following instability criterium is obtained:

$$(1 - m/2)\sqrt{2g\delta_0}\sqrt{\frac{\psi_0}{\beta}} < (1+n)c_0|E_0|. \tag{9}$$

It must be born in mind that this result only delivers a diagnosis of instability.

As it will be shown in Sections 6 and 7, when the state of reference is critical, the instability criterium expressed by (9) provides necessary conditions for roll waves to form.

When δ is an increasing function of h, i.e. E is positive, only one condition remains. That is the case for two-dimensional flows as $\delta = 4h$ and $c = (gh)^{1/2}$, so that (9) provides $\frac{1+n}{2-m}\left(\frac{8\beta}{\psi_0}\right)^{1/2} > 1$, and when the regime is rough, the well-known condition $2(1+n)^2\beta > \psi_0$ is recovered (Dressler, 1949).

For any cross-section and h_0 close to zero, (9) is reduced to $(\frac{\beta}{2\psi_0})^{1/2} > \frac{3}{8}\frac{(2-m)}{(1+n)}$.

For h_0 close to $\tilde{h}$, $E_0 \simeq 0$ and the flow is unconditionally stable.

On the contrary, when $h_0 > \tilde{h}$, E_0 is negative and the condition is fulfilled for h close to H as $E \to -\infty$: therefore, when the duct is almost filled, the flow is unstable.

3.2. Influence of flow regime

All previous results may be plotted in the $\frac{h_0}{H}$, $(\frac{\psi_0}{\beta})^{1/2}$ plane. As the flow regime is to be taken into account, the representation must involve the characteristic Reynolds number $Re = \frac{u_0\delta_0}{\nu} = \frac{\delta_0}{\nu}(2g\delta_0\frac{\beta}{\psi_0})^{1/2}$.

Let Re_L be the transitional value of Re between laminar and smooth turbulent regimes and Re_T the value separating the two turbulent regimes. Obviously, smooth turbulent flows are observed when $Re_L\sqrt{\frac{\psi_0}{\beta}} < \frac{\delta_0}{\nu}\sqrt{2g\delta_0} < Re_T\sqrt{\frac{\psi_0}{\beta}}$.

Calculations have been performed for a circular duct of radius R. With the help of formulae given at the end of Section 2 the instability criterium (9) becomes $\sqrt{\frac{\psi_0}{\beta}} < \frac{2(1+n)}{2-m}\frac{|\sin 2\theta - 2\theta\cos 2\theta|}{(2\theta\sin\theta)^{3/2}}$. As for the Reynolds number, $Re = \frac{R}{\nu}(2gR\frac{\beta}{\psi_0})^{1/2}(\frac{2\theta-\sin 2\theta}{\theta})^{3/2}$. Consequently, the transition between the two turbulent regimes is represented in the θ, $(\frac{\psi_0}{\beta})^{1/2}$ plane by the curve $\sqrt{\frac{\psi_0}{\beta}} = \frac{(2gR^3)^{1/2}}{\nu Re_T}(\frac{2\theta-\sin 2\theta}{\theta})^{3/2}$.

A similar formula, with Re_T replaced by Re_L, holds for the transition from laminar to smooth turbulent regime.

Fig. 3 represents the domains where the flow is stable and unstable, together with transition curves corresponding to a duct of radius $R = 0.0125$ m, to water and to the conventional values $Re_L = 1500$ and $Re_T = 50000$. The radius R only interferes in the values of the Reynolds number: it has been chosen in relation with the experimental validation presented in Section 8.1. In the

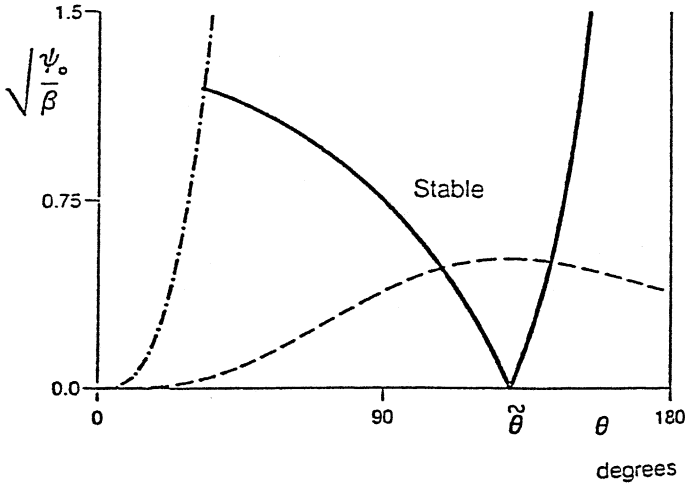

Fig. 3. Stability diagram for circular ducts, with $m = 0$, $n = 1/3$ for rough turbulent flow. The curves concerning Re_L and Re_T correspond to water and $R = 0.0125$ m: — neutral stability; $-\cdot- Re_L = 1.5 \times 10^3$; $--- Re_T = 5 \times 10^4$.

region of smooth turbulent flow, $m = n = 0.2$ has been set, whereas in the rough turbulent region $m = 0$ and $n = 1/3$. It has been checked that the neutral stability curve is almost the same for $n = 0$ and $n = 1/3$.

4. Discontinuities of finite amplitude

We recall hereafter the main properties concerning discontinuities of finite amplitude which have been brought to evidence recently (Dyment, 1998). Consider a stationary jump in a steady flow. The velocity and height are u_0 and h_0 upstream and u and h downstream. The equations of conservation of mass and momentum give

$$\frac{u_0}{f_0} = \frac{u}{f} = \left(-g\frac{\varphi - \varphi_0}{f - f_0} \right)^{1/2}, \tag{10}$$

and since the variation in energy cannot be positive, $h \geqslant h_0$ is obtained, resulting from $D > 0$. As a consequence $u_0 \geqslant c_0$ and $u \leqslant c$ hold: so the velocity is supercritical upstream and subcritical downstream.

Thus, qualitatively, all results valid in rectangular channels are generalized for conduits of round shaped cross-section.

According to (10), h is an increasing function of u_0. For a certain value of u_0 given by (10) with ϕ and F in place of φ and f, the top of the conduit is reached downstream and a plug is formed: that is an incipient choked discontinuity.

When u_0 is larger, that is

$$\frac{u_0}{f_0} > \left(-g\frac{\phi - \varphi_0}{F - f_0} \right)^{1/2}, \tag{11}$$

the discontinuities are choked. By contrast, discontinuities with $h < H$ will be called free.

Let $\rho g(H - z) + P$ be the pressure inside the plug: the pressure at the top, P, is merely induced because the liquid is impeded to spread vertically. The conservation of mass and momentum leads to (Dyment, 1998)

$$\frac{P}{\rho F} = \frac{u_0^2}{f_0^2}(f_0 - F) - g(\phi - \varphi_0) = \frac{U^2}{F^2}(f_0 - F) - g(\phi - \varphi_0), \tag{12}$$

with P positive due to (11).

Similarly to free discontinuities, the flow is still supercritical upstream and, as $c \to \infty$ when $h \to H$, it is subcritical downstream.

It can easily be deduced from (12) that for a given value of $u_0 \frac{\mathrm{d}P}{\rho F \,\mathrm{d}h_0} = b_0(c_0^2 - u_0^2)$, so that P is a decreasing function of h_0, tending to infinity when h_0 tends to zero. Using expansions, we obtain for $h_0 \ll H$, i.e. $u_0^2 > g\phi f_0$: $P = \frac{2\rho u_0^2}{3A} h_0 b_0$.

The results summarized in this section represent an important breakthrough for the investigation of all flows containing hydraulic discontinuities. Particularly, the property stating that, in round conduits, particles crossing a discontinuity cannot undergo a decrease in height, is of great importance. Previously, as long as the shape of the cross-section was not specified, jumps

accompanied by a rise or a fall on the liquid level could be anticipated according to the sign of D, though the occurrence of D negative is rare (Dyment, 1998). Henceforth this ambiguousness is removed, which will make easier the study of roll waves and slugs undertaken in what follows.

5. Periodic waves containing bores

5.1. Flow in the liquid layer

We intend to construct wave solutions containing periodic structures propagating with a constant speed ω. Therefore $x - \omega t = \xi$ becomes the single variable, the flow being steady in the frame of reference accompanying the waves.

In what follows, the waves will be termed travelling downward/upward according to the direction of propagation with respect to the moving liquid and, progressive/regressive when the fixed reference is considered.

Eq. (4) integrates to give

$$(\omega - u)a = q. \tag{13}$$

As defined by (13), q is the opposite of the relative discharge. The discharge q may be positive or negative according to whether ω is larger or smaller than u. However, u being positive as the fluid is supposed flowing downwardly, we must have $\omega > \frac{q}{a}$.

Eq. (5) becomes

$$\left(1 - \frac{q^2}{a^2 c^2}\right)\frac{\mathrm{d}h}{\mathrm{d}\xi} = \beta - \frac{\psi}{2g\delta}\left(\omega - \frac{q}{a}\right)^2, \tag{14}$$

where the left-hand side is simply $\frac{\mathrm{d}}{\mathrm{d}\xi}\left(h + \frac{q^2}{2ga^2}\right)$.

As a, c, δ and ψ are constant for a given value of h, Eq. (14) provides a definite value of $\frac{\mathrm{d}h}{\mathrm{d}\xi}$, which means that h is monotonous, a result inconsistent with a continuous periodic wavy solution. Thereby, a discontinuity exists at one end of every unit structure and consequently critical conditions exist too. The critical height, say h^*, is unique because D is positive (Dyment, 1981). From Section 4, we know that h^* lies between the upstream and downstream heights of the bore, h_1 and h_2, h_2 being equal to H when the bore is choked. We have $q^2 = a^{*2}c^{*2}$ and as in any critical section the left-hand side of Eq. (14) cancels, the same occurs for the right-hand side: so, β must be positive, as might be foreseen, and $\left(\omega - \frac{q}{a^*}\right)^2 = u^{*2}$ where u^* is the uniform flow velocity under critical conditions, defined by formula (7):

$$u^* = \left(\frac{2g\delta^*\beta}{\psi^*}\right)^{1/2}. \tag{15}$$

Unambiguously,

$$\omega = \frac{q}{a^*} + u^* \tag{16}$$

is obtained because $u = \omega - \frac{q}{a}$ is positive since downflows are considered.

Thanks to (15), (16) and (8), Eq. (14) becomes

$$\left(1-\frac{a^{*^2}c^{*^2}}{a^2c^2}\right)\frac{\mathrm{d}h}{\beta\,\mathrm{d}\xi}=\mathscr{S}, \tag{17}$$

with

$$\mathscr{S}=1-\left(\frac{\delta^*}{\delta}\right)^{1+n}\left(\frac{u}{u^*}\right)^{2-m}. \tag{18}$$

According to (15) the function $\mathscr{S}$ depends on two parameters, h^* and $\sqrt{\frac{\psi^*}{\beta}}$.

As previously explained h is a monotonous function of ξ. The sign of $\frac{\mathrm{d}h}{\mathrm{d}\xi}$ will be prescribed by the jump condition $h_2>h_1$. On the other hand the sign of $1-\frac{a^{*^2}c^{*^2}}{a^2c^2}$ is the same than that of $h-h^*$ because, thanks to (2), $\frac{\mathrm{d}}{\mathrm{d}h}\left(1-\frac{a^{*^2}c^{*^2}}{a^2c^2}\right)=\frac{a^{*^2}c^{*^2}}{2g}D$ is positive. Finally, $\frac{\mathrm{d}h}{\mathrm{d}\xi}$ and $(h-h^*)\mathscr{S}$ must have the same sign.

Two cases can be encountered depending on the sign of q. They will be analyzed in detail in Sections 6 and 7.

5.2. Flow across free and choked discontinuities

Let us now express the relations to be satisfied across a free discontinuity.

For a downward travelling bore, Eqs. (10) give $\frac{\omega-u_1}{f_1}=\frac{\omega-u_2}{f_2}=\left(g\frac{\varphi_2-\varphi_1}{f_1-f_2}\right)^{1/2}$ so that, taking $(\omega-u_1)a_1=(\omega-u_2)a_2=a^*c^*$ into account,

$$g(\varphi_2-\varphi_1)=a^{*^2}c^{*^2}(f_1-f_2) \tag{19}$$

can be deduced.

For an upwardly travelling bore, we have $\frac{u_1-\omega}{f_1}=\frac{u_2-\omega}{f_2}=\left(g\frac{\varphi_2-\varphi_1}{f_1-f_2}\right)^{1/2}$ and $(u_1-\omega)a_1=(u_2-\omega)a_2=a^*c^*$, with the result that (19) still holds.

Thanks to (1), Eq. (19) can be written

$$\frac{f_2-f_1}{\varphi_2-\varphi_1}=\left(\frac{\mathrm{d}f}{\mathrm{d}\varphi}\right)^*. \tag{20}$$

Thereby, the straight line joining the points representative of the upstream and downstream of the discontinuity is parallel to the tangent drawn at the point corresponding to the critical state (Fig. 4). As a consequence, the condition for free discontinuity occurrence is $\varphi_1>\varphi_i$, φ_i being the upstream value of φ_1 when $\varphi_2=\phi$, defined by

$$g\frac{\phi-\varphi_i}{F-f_i}=-a^{*^2}c^{*^2}. \tag{21}$$

As φ_i and f_i are the values of φ and f yielding the incipient choked discontinuity corresponding to the critical height h^*, for $\varphi_1<\varphi_i$ the discontinuity is choked.

It is obvious from Fig. 4 that φ_i is an increasing function of φ^*.

For small values of h_i, Eq. (21) becomes

$$g\phi b_i^3=3R_{\mathrm{B}}a^{*^2}c^{*^2}. \tag{22}$$

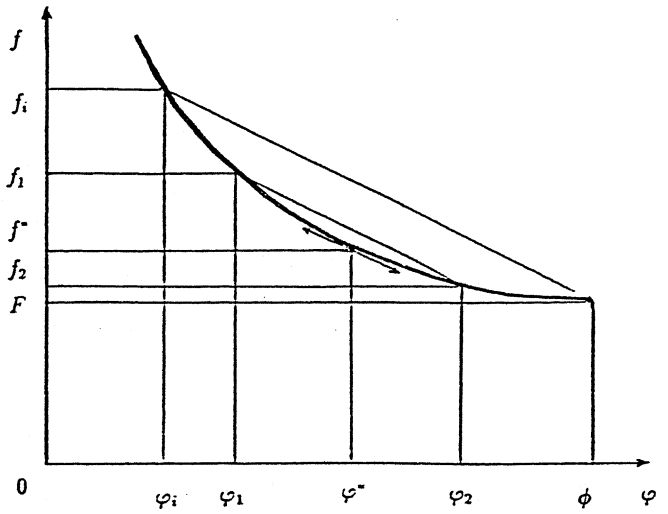

Fig. 4. Free bores for given critical height: $\varphi_i < \varphi_1 < \varphi^*$.

When h^* itself is small,

$$9R_B^2\phi b_i^3 = b^{*8}. \tag{23}$$

At the top, $h_i = h^* = H$, and in the vicinity of the top, an expansion provides

$$2b_i = 3b^*. \tag{24}$$

For a circle, the relation between θ_i and θ^* expressed by (21) is drawn in Fig. 5. As for relations (22)–(24) they become $\theta_i^3 = \frac{3\pi}{2}\left(\frac{a^*}{\frac{\pi R^2}{2}}\right)^2 \frac{c^{*2}}{gR}$, $\theta_i^3 = \frac{2}{9\pi}\theta^{*8}$ and $2\theta_i = 3\theta^* - \pi$.

Let us come now to choked bores.

For a downwardly propagating bore, conservation of mass allows to write $(\omega - U)A = a^*c^*$, U being the velocity inside the liquid plug. Then

$$\omega = U + \frac{c^*F}{f^*}. \tag{25}$$

For an upwardly propagating bore, $(U - \omega)A = a^*c^*$, and

$$\omega = U - \frac{c^*F}{f^*}. \tag{26}$$

In both cases, according to (12), just at the top of the plug, the downstream pressure P is given by

$$\frac{P}{\rho F} = a^{*2}c^{*2}(f_1 - F) - g(\phi - \varphi_1). \tag{27}$$

Thanks to (1), this relation may be written

$$F - f_1 = \left(\phi + \frac{P}{\rho g F} - \varphi_1\right)\left(\frac{\mathrm{d}f}{\mathrm{d}\varphi}\right)^*. \tag{28}$$

According to (27), P is an increasing function of h^* and a decreasing function of h_1.

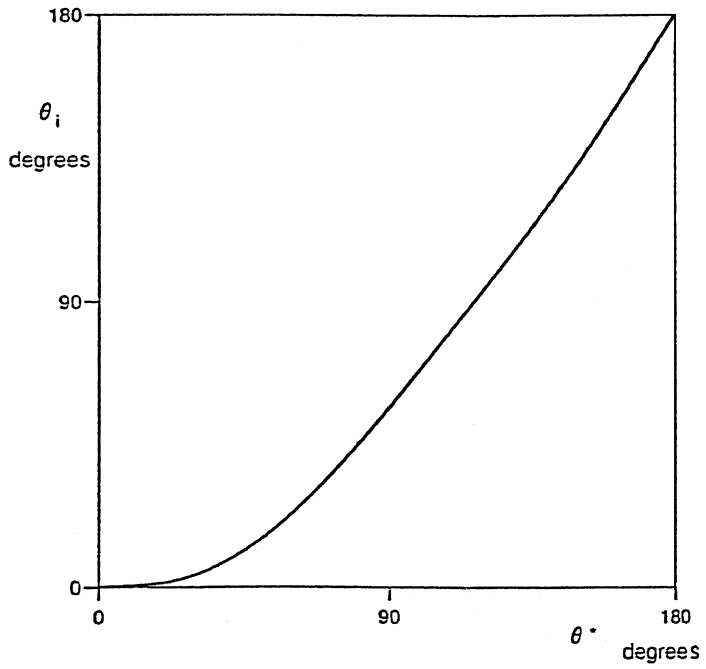

Fig. 5. The relation between critical and incipient choked discontinuity conditions for circular ducts.

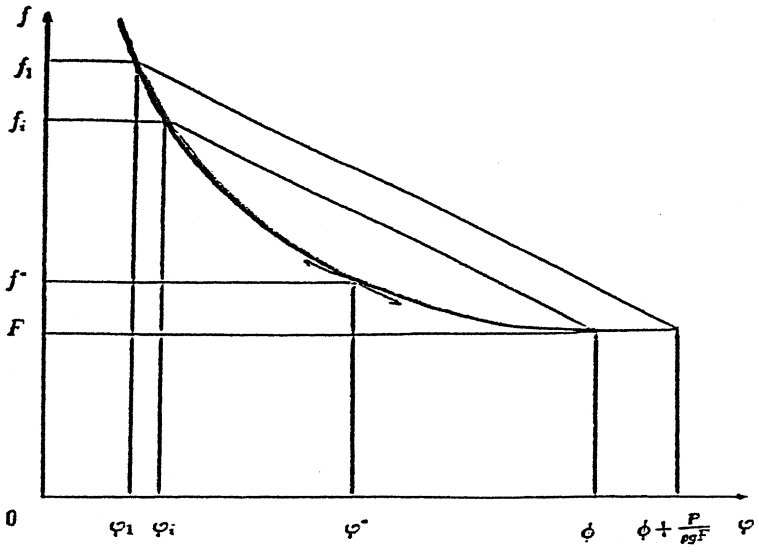

Fig. 6. Choked bores for given critical height: $\varphi_1 < \varphi_i < \varphi^*$.

The comparison between formulae (20) and (28) shows that a diagram similar to that of Fig. 4 can be drawn, f_2 being replaced by F and φ_2 by $\phi + \frac{P}{\rho g F}$ (Fig. 6).

It follows from all previous results illustrated in Figs. 4 and 6, that roll waves occur for $\varphi_i < \varphi_1 < \varphi^*$ and slugs for $\varphi_1 < \varphi_i < \varphi^*$.

All properties brought to evidence in this section will now be used in order to investigate successively downwardly and upwardly propagating waves.

6. Downwardly travelling waves

6.1. Necessary conditions for the existence of downward roll waves

In this section, we consider downwardly travelling waves corresponding to $q = a^* c^*$, which involves $\omega > u$ according to (13). Then, Eq. (16) provides

$$\omega = u^* + c^*, \tag{29}$$

and when reported in (13),

$$u = u^* + c^* \frac{(a - a^*)}{a}. \tag{30}$$

Consequently, (18) and (15) lead to

$$\mathscr{S} = 1 - \left(\frac{\delta^*}{\delta}\right)^{1+n} \left[1 + \frac{c^*}{\sqrt{2g\delta^*}} \sqrt{\frac{\psi^*}{\beta}} \left(1 - \frac{a^*}{a}\right)\right]^{2-m}. \tag{31}$$

In the frame of reference accompanying the waves, the fluid moves from the right to the left, and as h_2 must be larger than h_1, we have $\frac{\mathrm{d}h}{\mathrm{d}\xi} > 0$.

When expanded in the vicinity of h^*, Eq. (17) becomes

$$\frac{a^{*2} c^{*2} \delta^* D^*}{2g\beta} \frac{\mathrm{d}h}{\mathrm{d}\xi} = (1+n)E^* - (2-m)\frac{g\delta^*}{u^* c^*}. \tag{32}$$

As $\frac{\mathrm{d}h}{\mathrm{d}\xi}$ is positive, we must have $E^* > 0$, so that the necessary condition

$$h^* < \tilde{h} \tag{33}$$

must be satisfied. The right-hand side of (32) must be positive, hence, as might be expected, the instability condition for $h^* < \tilde{h}$ found in Section 3.1, is recovered, the state of reference being the critical one. Taking (15) into account, we obtain

$$\sqrt{\frac{\psi^*}{\beta}} < \frac{(1+n)}{(1-m/2)} \frac{c^*}{\sqrt{2g\delta^*}} E^*. \tag{34}$$

Let us now inspect what happens when h is far from h^*, bearing in mind that $\frac{\mathrm{d}h}{\mathrm{d}\xi} > 0$ implies $(h - h^*)\mathscr{S} > 0$.

When $h < h^*$, $\mathscr{S}$ must be negative. Now, for $h < h^*$ we have $u < u^*$, according to (30). As a consequence, δ must necessarily be smaller than δ^*, which is consistent with $h < h^*$.

When $h > h^*$, $\mathscr{S}$ must be positive. Here $u > u^*$, so that $\delta > \delta^*$ is necessary. Bearing in mind that when h^* is larger than h_Δ, a second value h^*_δ exists which is such that $\delta = \delta^*$. If $h^* < h_\Delta$, the

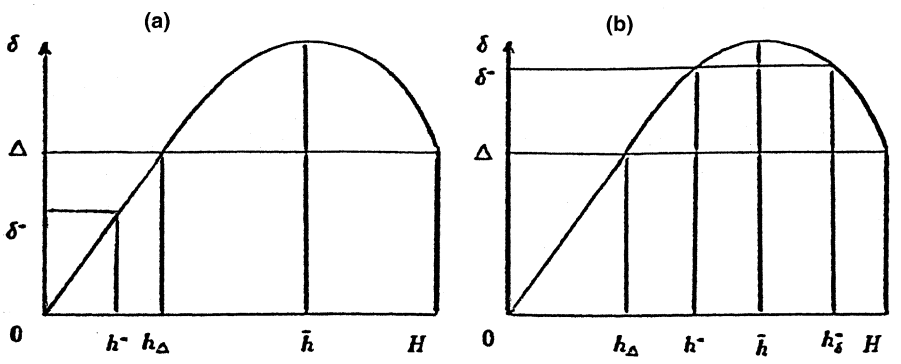

Fig. 7. Downwardly travelling waves. (a) $h^* < h_\Delta$; possible slug flow; (b) $h^* > h_\Delta$; no slug flow.

condition $\delta > \delta^*$ is fulfilled (Fig. 7a). If $h^* > h_\Delta$, which only holds in the interval (h^*, h_δ^*), roll waves cannot reach the top of the duct (Fig. 7b).

Indeed, the solution cannot exist over the whole height of the duct. Let (h_I, h_S) be the interval where the waves can occur: h_I is the highest root of equation $\mathscr{S} = 0$ below h^* and h_S is the lowest root above h^*.

The derivative of $\mathscr{S}$ is

$$\frac{\mathrm{d}\mathscr{S}}{\mathrm{d}h} = \frac{(1+n)c^*a^*}{\delta^* u^* a}\left(\frac{\delta^*}{\delta}\right)^{2+n}\left(\frac{u}{u^*}\right)^{1-m}\left[\frac{auE}{a^*c^*} - 4\frac{(2-m)b}{(1+n)k}\right].$$

At $h = h^*$, $\mathscr{S}$ is zero and $\frac{\mathrm{d}\mathscr{S}}{\mathrm{d}h}$ is positive according to (34). The curve representative of $\mathscr{S}$ versus h starts at the value h_U where u vanishes: it is defined by $\frac{a_U}{a^*} = \frac{c^*}{u^*+c^*}$ so that $h_U < h^*$ (Fig. 8).

At $h = h_U$, we have $\mathscr{S} = 1$ and $\frac{\mathrm{d}\mathscr{S}}{\mathrm{d}h} = 0$. Consequently, the root h_I always exists and it is situated between h_U and h^*. Consider the roots of the expression between brackets in $\frac{\mathrm{d}\mathscr{S}}{\mathrm{d}h}$, defined by $E = \frac{4(2-m)a^*c^*b}{(1+n)kau}$. From what precedes, there is one root between h_I and h^*. As au and $\frac{k}{b}$ are increasing functions of h, $\frac{b}{kau}$ decreases from infinity at h_U to zero at H, and then, owing to the known variations of E, there is necessarily a second root larger than h^*. Consequently, $\mathscr{S}$ may cancel only once for h larger than h^*, say at $h = h_S$ (Fig. 8). When h_S does not exist slug flow is possible. At $h = H$, we have $\frac{\mathrm{d}\mathscr{S}}{\mathrm{d}h} \to -\infty$ and at $h = \tilde{h}$, $\frac{\mathrm{d}\mathscr{S}}{\mathrm{d}h}$ is negative.

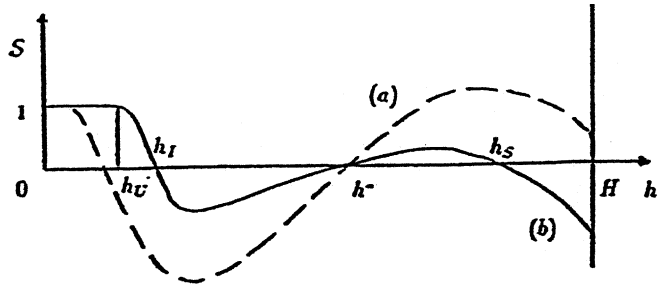

Fig. 8. Variation of $\mathscr{S}$ for downwardly travelling waves: (a) – – – possible slug flow; (b) — no slug flow. $\frac{\psi}{\beta}$ is smaller for (a) than for (b).

The variation of $\mathscr{S}$ in terms of $\frac{\psi^*}{\beta}$ depends on the derivative with respect to this parameter, which may easily be expressed from (31). This derivative and $h - h^*$ have like signs, therefore $\mathscr{S}$ increases with $\frac{\psi^*}{\beta}$ for $h < h^*$ and decreases for $h > h^*$. In particular, the root h_I increases with $\frac{\psi^*}{\beta}$ (Fig. 8).

Roll waves take place if $h_1 > h_I$ and $h_1 > h_i$ (Fig. 4). According to (17), one among the smooth portions of the free surface is represented by $\beta\xi = \int_H^h (1 - \frac{a^{*2}c^{*2}}{a^2c^2}) \frac{\mathrm{d}h}{\mathscr{S}}$, the origin of ξ being taken at $h = H$. The wavelength L is given by $\beta L = \int_{h_1}^{h_2} (1 - \frac{a^{*2}c^{*2}}{a^2c^2}) \frac{\mathrm{d}h}{\mathscr{S}}$.

6.2. Necessary conditions for the existence of downward slugs

Slug flow is possible if the crests of the roll waves may reach the top of the duct, namely in case of Fig. 7a, that is for

$$h^* < h_\Delta. \tag{35}$$

Starting from a case when $\mathscr{S}(H) < 0$ (Fig. 8, curve b), slugs may be obtained by decreasing $\frac{\psi^*}{\beta}$ in order to yield $\mathscr{S}(H)$ positive. Obviously, it results from Fig. 6 that slugs may exist only when h_1 is smaller than h_i. However, as h_1 must be larger than h_I the necessary condition

$$h_i > h_I \tag{36}$$

is to be fulfilled. For a given value of h^* the interval (h_I, h_i) decreases with increasing $\frac{\psi^*}{\beta}$ since h_I increases whereas h_i remains constant.

As $\mathscr{S}(H)$ must be positive for $h^* \leqslant h \leqslant H$, no root h_s exists and the necessary condition $\mathscr{S}(H) > 0$ is required, i.e.

$$\left(\frac{\Delta}{\delta^*}\right)^{\frac{1+n}{2-m}} - 1 > \frac{c^*}{u^*}\left(1 - \frac{a^*}{A}\right). \tag{37}$$

The properties of both jumps and smooth profiles of the interface can be gathered because the variation of $\mathscr{S}$ versus φ and h are similar as $\frac{\mathrm{d}\mathscr{S}}{\mathrm{d}h} = a\frac{\mathrm{d}\mathscr{S}}{\mathrm{d}\varphi}$. The resulting global diagram for slug flow is presented in Fig. 9.

The pressure in the gaseous bubble being zero and the pressure gradient along the duct being negligible, the pressure P behind the discontinuity is balanced by the frictional resistance loss

$$P = \left(g\beta - \frac{\Psi U^2}{2\Delta}\right)\rho L_\mathrm{p}, \tag{38}$$

where Ψ is the friction factor of the plug flow and L_p the length of the plug.

The elimination of P between (27) and (38) leads to

$$\frac{c^{*2}}{f^{*2}}(f_1 - F) - g(\phi - \varphi_1) = \left(g\beta - \frac{\Psi U^2}{2\Delta}\right)\frac{L_\mathrm{p}}{F}. \tag{39}$$

The velocity U is obtained from (30):

$$U = u^* + c^*\left(1 - \frac{F}{f^*}\right). \tag{40}$$

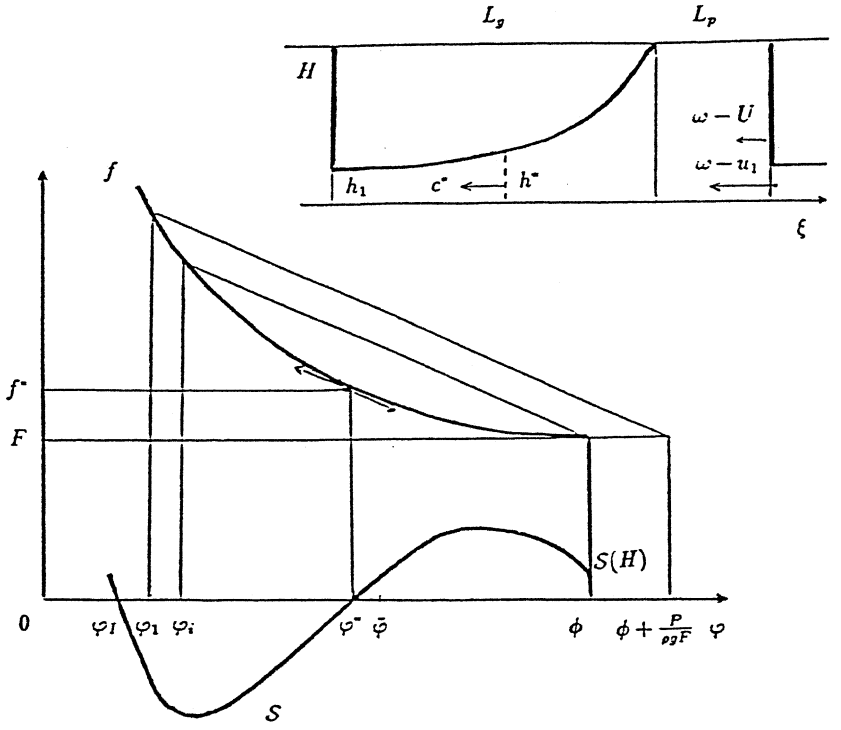

Fig. 9. Global diagram for downward slug flows: $\varphi_I < \varphi_1 < \varphi_i$, $\mathscr{S}(H) > 0$.

The jump is situated at the rear of the gaseous bubble and it moves faster than the liquid inside the plug.

The conservation of mass for both liquid and gas is expressed by $au + (A - a)v = AU$. Taking (30) and (40) into account $v = \omega$ is obtained: the gas velocity is everywhere equal to the speed of propagation. The comparison with (30) shows that the gas moves faster than the liquid.

The friction factors Ψ and ψ^* are connected by a relation similar to (8),

$$\frac{\Psi}{\psi^*} = \left(\frac{u^*}{U}\right)^m \left(\frac{\delta^*}{\Delta}\right)^n, \tag{41}$$

which allows to transform (38) into $P = [1 - (\frac{\delta^*}{\Delta})^{1+n}(\frac{U}{u^*})^{2-m}]\rho g \beta L_p$.

Therefore, P is connected to the expression of the function $\mathscr{S}$ at the junction between the plug and the smooth profile of the interface:

$$P = \rho g \beta L_p \mathscr{S}(H). \tag{42}$$

Then, thanks to (17), $\frac{P}{\rho g L_p}$ is equal to the slope $\frac{dh}{d\xi}$ at $h = H$.

Afterwards, with the help of (15), (39) and (41), L_p can be expressed in terms of h^*, $\frac{\psi^*}{\beta}$ and h_1:

$$\beta L_p \left\{ 1 - \left(\frac{\delta^*}{\Delta}\right)^{1+n} \left[1 + \frac{c^*}{\sqrt{2g\delta^*}} \sqrt{\frac{\psi^*}{\beta}} \left(1 - \frac{F}{f^*}\right) \right]^{2-m} \right\} = \frac{Fc^{*2}}{gf^{*2}}(f_1 - F) - F(\phi - \varphi_1). \tag{43}$$

Concerning the bubble length L_g, it is deduced from the expression of L for roll waves, h_2 being replaced by H:

$$\beta L_g = \int_{h_1}^{H} \left(1 - \frac{a^{*2} c^{*2}}{a^2 c^2}\right) \frac{\mathrm{d}h}{\mathscr{S}}. \tag{44}$$

The wavelength is $L = L_g + L_p$ and the frequency is equal to $\frac{u^* + c^*}{L_p + L_g}$.

It has been seen in Section 4 that P is a decreasing function of h_1, so that the same holds for L_p according to (38). Besides, formula (43) indicates that L_p increases with $\sqrt{\frac{\psi^*}{\beta}}$.

For given h^* and $\sqrt{\frac{\psi^*}{\beta}}$, the maximum of P and L_p is obtained when $h_1 = h_I$, as can easily be checked in Fig. 9. Then, according to (17), the slope of the interface is zero upstream of the jump.

The solution is simplified when h^* is small enough to provide a steep slope of the curve representative of f in Fig. 9 at $\varphi = \varphi^*$. Then, according to (21) the height h_i is very small and (22) can be used, with the pressure P given by the last formula of Section 4, where u_0 is to be replaced by $\omega - u_1 = \frac{a^* c^*}{a_1}$, providing $P = \frac{3\rho a^{*2} c^{*2}}{2A(2R_B h_1^3)^{1/2}}$.

6.3. The domain of downward slug occurrence

The domain of downward slug flows in the plane of parameters h^* and $\sqrt{\frac{\psi^*}{\beta}}$ must be situated under the neutral stability curve corresponding to (34), that is

$$\sqrt{\frac{\psi^*}{\beta}} = \frac{1+n}{2-m} E^* \frac{c^*}{\sqrt{2g\delta^*}}. \tag{45}$$

For very low $\frac{\psi^*}{\beta}$, h_I tends to zero, $\mathscr{S}$ is almost equal to $1 - (\frac{\delta^*}{\Delta})^{1+n}$ and so it is positive for $h > h^*$ since $h^* < h_\Delta$. Therefore, the condition $\mathscr{S}(H) > 0$ is fulfilled and slug flow may exist. When $\frac{\psi^*}{\beta}$ is increased at given h^*, h_i remains unchanged, whereas $\mathscr{S}(H)$ decreases and h_I increases, hence occurrence of slug flow disappears, either because $\mathscr{S}(H)$ becomes zero or because h_I becomes equal to h_i. Consequently, the domain of downward slugs is bounded by either the graph $\mathscr{S}(H) = 0$, with $P = 0$ according to (42), i.e. $h_1 = h_i$, or by the graph $h_I = h_i$, i.e. $\mathscr{S}(h_i) = 0$, as $\mathscr{S}(h_I)$ is zero by definition.

Taking (15) and (31) into account, we obtain respectively

$$\frac{c^*}{\sqrt{2g\delta^*}} \left(1 - \frac{a^*}{A}\right) \sqrt{\frac{\psi^*}{\beta}} = \left(\frac{\Delta}{\delta^*}\right)^{\frac{1+n}{2-m}} - 1 \tag{46}$$

and

$$\frac{c^*}{\sqrt{2g\delta^*}} \left(1 - \frac{a^*}{a_i}\right) \sqrt{\frac{\psi^*}{\beta}} = \left(\frac{\delta_i}{\delta^*}\right)^{\frac{1+n}{2-m}} - 1, \tag{47}$$

h_i and h^* being connected by (21).

The neutral stability curve is already known. It cuts the h^* axis at $\tilde{h}$, and the $\sqrt{\frac{\psi^*}{\beta}}$ axis at $\frac{\sqrt{8}}{3} \frac{1+n}{1-m/2}$.

The curve relative to the condition at the top cuts the $\sqrt{\frac{\psi^*}{\beta}}$ axis at h_Δ and when h^* tends to zero $\sqrt{\frac{\psi^*}{\beta}} = (\frac{24\Delta}{h^*})^{\frac{1+n}{1-m/2}} \to \infty$ is obtained.

The last curve, Eq. (47), can cut the $\sqrt{\frac{\psi^*}{\beta}}$ axis only at the origin because elsewhere $\delta_i = \delta^*$ is not possible. Close to the origin and with the help of (23), an expansion gives $\sqrt{\frac{\psi^*}{\beta}} = \frac{16}{9\phi}(R_B h^{*5})^{1/2}$.

Application is made to circular ducts with $m = 0$, $n = 1/3$ in Fig. 10. Roll waves are possible over the whole region beneath the neutral stability curve, whereas slug flow can occur only within the domain DS where $\mathscr{S}$ is positive and h_I smaller than h_i. The longest plug and highest overpressure correspond to $h_1 = h_I$. The widest interval for slug occurrence is obtained for θ^* close to 81° and it extends up to $\sqrt{\frac{\psi^*}{\beta}} \simeq 0.32$. Consider $\frac{u^*}{c^*} = \sqrt{\frac{8\sin\theta^*\beta}{\theta^*\psi^*}}$. As $0 < \theta^* < 90°$, $\sqrt{\frac{8\sin\theta^*}{\theta^*}}$ is higher than 2.26, a value obtained for 90°, and since $\sqrt{\frac{\psi^*}{\beta}}$ is lower than 0.32, $\frac{u^*}{c^*}$ is higher than 7.05. As a result, ω is very close to u^*. Similarly, according to (25), ω is not far from U since the difference $\omega - U = \frac{a^* c^*}{A}$ is lower than $0.44\sqrt{gR}$. Therefore, for downward slugs, the velocity inside the plug is close to the speed of propagation.

The inequality $h_1 < h_i$ allows to infer further information. Obviously, h_1 must be lower than the highest possible value of h_i. Now, as h_i increases with h^*, the maximum of h_i is reached at $\theta^* = 90°$ (Fig. 10), yielding $\theta_i = 56.6°$ thanks to (21), whence $\frac{h_i}{2R} = 0.225$. Therefore, $\frac{h_1}{2R}$ cannot exceed 0.225, which shows that downward slugs are of large amplitude.

Let us look at an example. Fig. 11a shows the smooth profiles of the interface, with $m = 0$, $n = \frac{1}{3}$, for $\theta^* = 75°$ and three values of $\sqrt{\frac{\psi^*}{\beta}}$ belonging to the instability domain of formula (34). On the left, the curves end at $h = h_I$. We have $\frac{h_I^*}{2R} = 0.37$, $c^* = 0.74\sqrt{gR}$, and $\theta_i = 38.5°$ is obtained from Eq. (21), i.e. $\frac{h_i}{2R} = 0.11$. The values of θ_I corresponding to $\sqrt{\frac{\psi^*}{\beta}}$ equal 0.1, 0.2 and 0.4 are approximately 25.6°, 34° and 47° (Fig. 11b). Therefore, θ_I is higher than θ_i for the highest value of $\sqrt{\frac{\psi^*}{\beta}}$. Roll waves exist when $\theta_i < \theta_1$ for $\sqrt{\frac{\psi^*}{\beta}} = 0.1$ and 0.2, and $\theta_I < \theta_1$ for $\sqrt{\frac{\psi^*}{\beta}} = 0.4$. Once θ_1 is

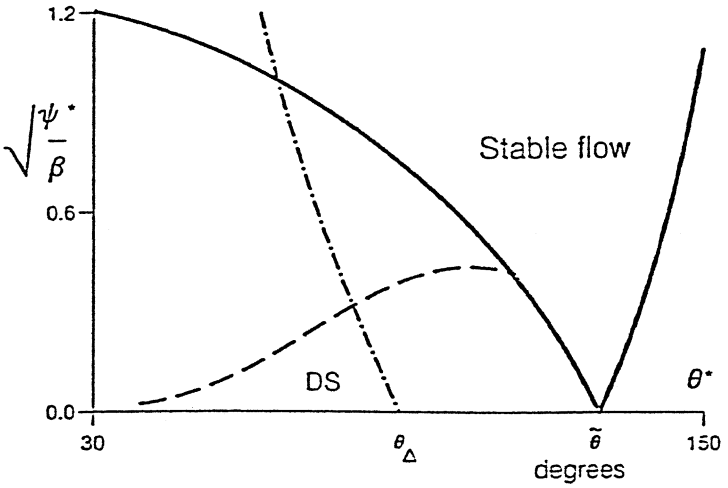

Fig. 10. Domain of downward slug flow occurrence DS in circular ducts for rough turbulent flow, $m = 0$, $n = 1/3$, $\theta_\Delta = 90°$, $\tilde{\theta} = 128.7°$: — neutral stability; $-\cdot-$ $\mathscr{S}(H) = 0$, Eq. (46); $---$ $\mathscr{S}(h_i) = 0$, Eq. (47).

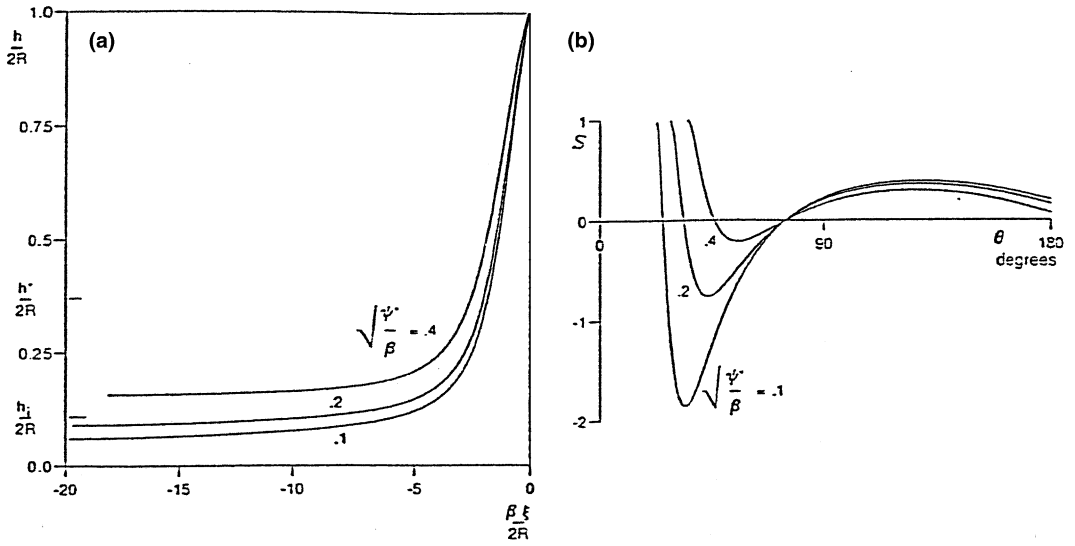

Fig. 11. Downward waves in circular ducts with $\theta^* = 75°$, rough turbulent flow $m = 0$, $n = \frac{1}{3}$ and three values of $\sqrt{\frac{\psi^*}{\beta}}$: (a) the smooth profile of the interface; (b) the function $\mathscr{S}$.

chosen, the angle θ_2 is obtained from relation (19). Then, $\frac{h_2}{2R}$ is known and the value of the wavelength can be read in Fig. 11a. Moreover, the speed of propagation ω is deduced from formula (29).

The representative point $\theta^* = 75°$, $\sqrt{\frac{\psi^*}{\beta}} = 0.2$ in Fig. 10 belongs to the domain of slugs, yielding $u^* = 8.99\sqrt{gR}$, $U = 9.49\sqrt{gR}$ and $\omega = 9.74\sqrt{gR}$ thanks to (15), (40) and (29). In this case $\theta_I = 34°$, so that θ_1 must lie between 34° and 38.5°. If $\theta_1 = 36°$ ($\frac{h_1}{R} = 0.19$) is chosen, the relations (27), (41) and (38) provide $P = 0.22\rho gR$, and $\beta L_p \simeq 1.38R$. The length L_g is deduced from Fig. 11a with $\beta L_g \simeq 27.26R$.

Obviously, the magnitude of all characteristic velocities is governed by the ratio ψ^*/β, since ω and U are close to u^*. In this connection it seems that ψ^*/β larger than about 0.04 is necessary in order to have no excessive values of the velocities. Thereby, in practice, the domain of downward slug occurrence of Fig. 10 is reduced to a narrow range corresponding approximately to $\psi^*/\beta > 0.04$ and $60° < \theta^* < 80°$.

A glance at the curves of Fig. 11a reveals that a large part of the interface is of almost constant height except close to the front where the slope of the interface is very steep, so that, on the whole, the gaseous bubble looks close to being symmetrical.

7. Upwardly travelling waves

7.1. Necessary conditions for the existence of upward waves

Let us consider now the second case, with $q = -a^*c^*$, which indicates that upwardly travelling waves are obtained, with $\omega < u$.

Relations (16) and (13) provide

$$\omega = u^* - c^*, \tag{48}$$

$$u = u^* - c^* \frac{a - a^*}{a}, \tag{49}$$

with the consequence that (18) becomes

$$\mathscr{S} = 1 - \left(\frac{\delta^*}{\delta}\right)^{1+n} \left[1 - \frac{c^*}{\sqrt{2g\delta^*}} \sqrt{\frac{\psi^*}{\beta}} \left(1 - \frac{a^*}{a}\right)\right]^{2-m}. \tag{50}$$

Contrary to the first case, here ω can be either positive, when $u^* > c^*$, with progressive waves, or negative, which corresponds to regressive waves occurring for $u^* < c^*$. These two kinds of waves are separated by steady flow configurations, $\omega = 0$, achieved for $u^* = c^*$: this relation represents

$$\sqrt{\frac{\psi^*}{\beta}} = \frac{\sqrt{2g\delta^*}}{c^*} \tag{51}$$

which decreases from $\sqrt{8}$ at $h^* = 0$, down to zero at $h^* = H$.

In the moving frame of reference the relative velocities are positive, and the jump condition $h_2 > h_1$ prescribes $\frac{\mathrm{d}h}{\mathrm{d}\xi} < 0$. Expanding Eq. (17) close to $h = h^*$ leads to $\frac{a^{*2}c^{*2}\delta^* D^*}{2g\beta} \frac{\mathrm{d}h}{\mathrm{d}\xi} = (1+n)E^* + (2-m)\frac{g\delta^*}{u^*c^*}$. The right-hand side must be negative, which implies $E^* < 0$, i.e.

$$h^* > \tilde{h}. \tag{52}$$

That expresses exactly the instability condition for $h^* > \tilde{h}$ found in Section 3.1, which may be written

$$\sqrt{\frac{\psi^*}{\beta}} < -\frac{(1+n)}{(1-m/2)} \frac{c^*}{\sqrt{2g\delta^*}} E^*. \tag{53}$$

For $h < h^*$, $\mathscr{S}$ must be positive. As u is a decreasing function of h, we have $u > u^*$ and consequently $\delta > \delta^*$ is necessary: this can only be fulfilled when h is higher than h_{δ^*}, the second value of h providing $\delta = \delta^*$.

When $h > h^*$, $\mathscr{S}$ must be negative. As $\frac{u}{u^*} < 1$, δ must be lower than δ^*, which is always the case up to H.

The derivative of $\mathscr{S}$ is

$$\frac{\mathrm{d}\mathscr{S}}{\mathrm{d}h} = \frac{(1+n)c^*a^*}{\delta^*u^*a} \left(\frac{\delta^*}{\delta}\right)^{2+n} \left(\frac{u}{u^*}\right)^{1-m} \left[\frac{auE}{a^*c^*} + \frac{4(2-m)b}{(1+n)k}\right].$$

At $h = h^*$, $\mathscr{S} = 0$ and $\frac{\mathrm{d}\mathscr{S}}{\mathrm{d}h} < 0$, whereas at $h = \tilde{h}$, $\frac{\mathrm{d}\mathscr{S}}{\mathrm{d}h} > 0$ and at $h = H$, $\frac{\mathrm{d}\mathscr{S}}{\mathrm{d}h} \to \infty$.

The sign of the derivative of $\mathscr{S}$ with respect to $\frac{\psi^*}{\beta}$ and of $h - h^*$ are alike, as it may easily be checked. Thereby, contrary to downwardly travelling waves, $\mathscr{S}$ decreases with increasing $\frac{\psi^*}{\beta}$ for $h < h^*$ and increases for $h > h^*$, so that the root h_I increases with $\frac{\psi^*}{\beta}$.

Upward roll waves are constructed by piecing together smooth profiles resulting from the integration of Eq. (17), $\mathscr{S}$ being now given by (50), with free discontinuities. The same conditions as for downward roll waves must hold for h_i, h_1 and h_I.

Concerning upwardly propagating slug flows, as in Section 6, they require h_1 to be smaller than h_i, the condition (37) to remain still valid and $\mathscr{S}(H)$ to be negative which means, thanks to (50):

$$1-\left(\frac{\Delta}{\delta^*}\right)^{\frac{1+n}{2-m}}>\frac{c^*}{u^*}\left(1-\frac{a^*}{A}\right). \tag{54}$$

A global diagram similar to that of Fig. 9 is to be used (Fig. 12) and the process indicated at the end of Section 6 in order to construct solutions still works, except that now h^* and $\sqrt{\frac{\psi^*}{\beta}}$ satisfy (48), (49), (52) and (53) instead of (29), (30), (33) and (34).

For upwardly travelling slugs the relation (38) is replaced by $P=(\frac{\Psi U^2}{2\Delta}-g\beta)\rho L_{\mathrm{p}}$ and (42) by $P=-\rho g\beta L_{\mathrm{p}}\mathscr{S}(H)$. The length of the plug is given by

$$\frac{c^{*2}}{f^{*2}}(f_1-F)-g(\phi-\varphi_1)=\left(\frac{\Psi U^2}{2\Delta}-g\beta\right)\frac{L_{\mathrm{p}}}{F}. \tag{55}$$

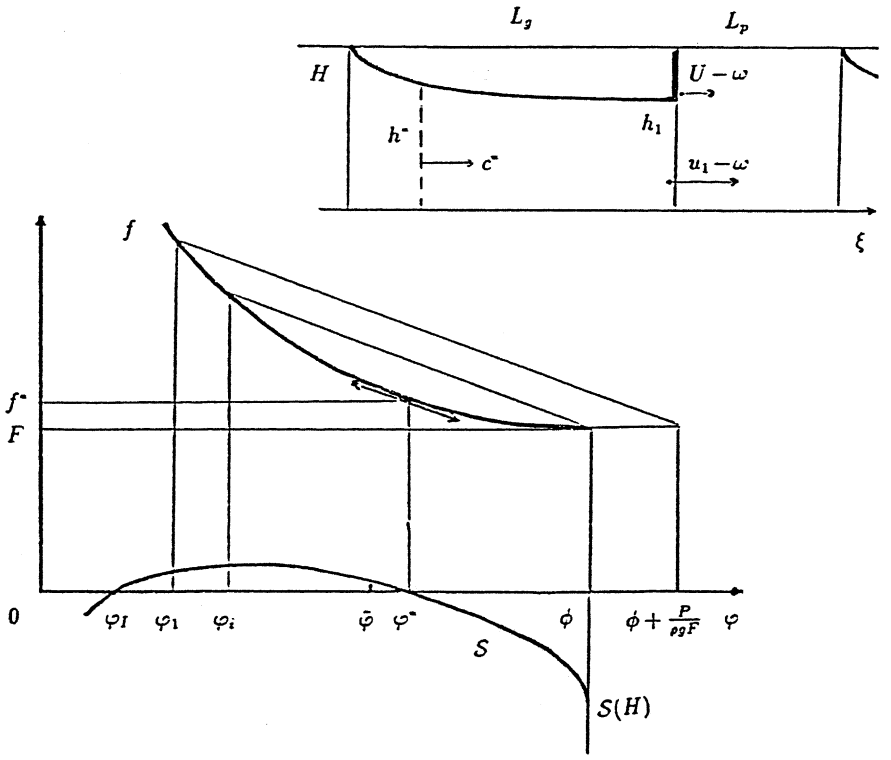

Fig. 12. Global diagram for upward slug flows: $\varphi_I<\varphi_1<\varphi_i$, $\mathscr{S}(H)<0$.

The relation (49) provides

$$U = u^* - c^*\left(1 - \frac{F}{f^*}\right). \tag{56}$$

The jump is situated at the front of the gaseous bubble and it moves slower than the liquid inside the plug.

By the method already used for downward slugs, the conservation of mass together with relations (49) and (56) lead to $v = \omega$. Therefore, the liquid moves faster than the gas.

The analog of formula (43) is

$$\beta L_{\mathrm{p}}\left\{\left(\frac{\delta^*}{\Delta}\right)^{1+n}\left[1 - \frac{c^*}{\sqrt{2g\delta^*}}\sqrt{\frac{\psi^*}{\beta}}\left(1 - \frac{F}{f^*}\right)\right]^{2-m} - 1\right\} = \frac{Fc^{*2}}{gf^{*2}}(f_1 - F) - F(\phi - \varphi_1).$$

The same trends as in Section 6.2 can be derived concerning the variation of P and L_{p}.

7.2. The domain of upward slug occurrence

Similarly to downwardly propagating waves, it may easily be shown that slugs exist for very small $\frac{\psi^*}{\beta}$ and that they disappear with increasing $\frac{\psi^*}{\beta}$, either because h_I becomes equal to h_i or because $\mathscr{S}(H)$ becomes positive. Thus, the domain of upward slug flow is bounded by the graphs of $\mathscr{S}(H) = 0$ and $\mathscr{S}(h_i) = 0$, the function $\mathscr{S}$ being now given by (50), with the result:

$$\frac{c^*}{\sqrt{2g\delta^*}}\left(1 - \frac{a^*}{A}\right)\sqrt{\frac{\psi^*}{\beta}} = 1 - \left(\frac{\Delta}{\delta^*}\right)^{\frac{1+n}{2-m}} \tag{57}$$

and

$$\frac{c^*}{\sqrt{2g\delta^*}}\left(1 - \frac{a^*}{a_i}\right)\sqrt{\frac{\psi^*}{\beta}} = 1 - \left(\frac{\delta_i}{\delta^*}\right)^{\frac{1+n}{2-m}}, \tag{58}$$

h_i and h^* being connected by (21).

The branch of the neutral stability curve starts at $\tilde{h}$ on the h^* axis and for $h^* \to H$, we have $\sqrt{\frac{\psi^*}{\beta}} = \frac{1+n}{1-m/2}\frac{\Delta R_{\mathrm{T}}}{\sqrt{8K}b^*} \to \infty$ as $b^* \to 0$.

As for downward slugs the curve defined by (57) cuts the $\sqrt{\frac{\psi^*}{\beta}}$ axis at h_Δ. When $h^* \to H$, an expansion gives $\sqrt{\frac{\psi^*}{\beta}} = 6\frac{1+n}{2-m}R_{\mathrm{T}}A\sqrt{\frac{2}{K^3b^{*3}}} \to \infty$.

Concerning the curve of Eq. (58), $\sqrt{\frac{\psi^*}{\beta}} \to 0$ is obtained for $\delta^* \to \delta_i$, which means that h^* coincides with h_i in this extreme case. This relation and (21) determine the corresponding value of h^*. When $\sqrt{\frac{\psi^*}{\beta}}$ becomes infinite, a^* tends to a_i, which is only possible for $h^* \to H$, and an expansion provides, with the help of (24), $\sqrt{\frac{\psi^*}{\beta}} = \frac{24}{19}\frac{1+n}{2-m}R_{\mathrm{T}}A\sqrt{\frac{2}{K^3b^{*3}}}$.

Taking into account $h_\Delta < \tilde{h} < h^*$ and the behaviour when h^* is close to H, it appears that the neutral stability curve lies above the curve of Eq. (58) and below that of Eq. (57). Consequently,

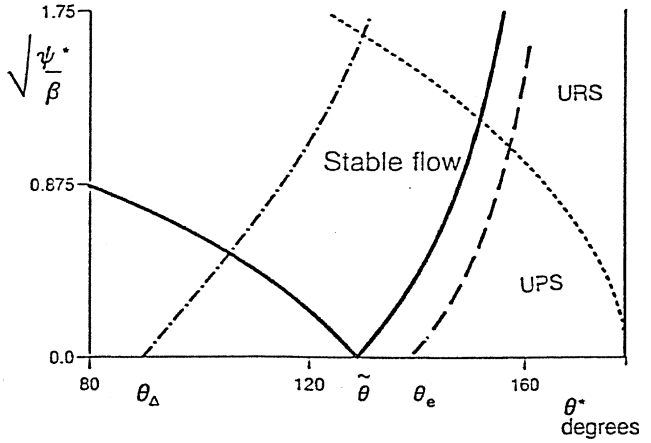

Fig. 13. Domain of upward slug floxv occurrence in circular ducts for rough turbulent flow, $m = 0$, $n = 1/3$, $\tilde{\theta} = 128.7°$, $\theta_e = 138°$: — neutral stability; $-\cdot-$ $\mathscr{S}(H) = 0$, Eq. (57); $---$ $\mathscr{S}(h_i) = 0$, Eq. (58); - - - - $u^* = c^*$.

in the domain of instability corresponding to $h^* > \tilde{h}$, $\mathscr{S}(H)$ cannot be positive, so that only situations when $\mathscr{S}$ remains negative from h^* up to H can occur.

Previous statements are corroborated when circular ducts are considered (Fig. 13). The curve corresponding to the condition to be fulfilled at H lies entirely in a region already forbidden by the instability condition.

Concerning the curve $\mathscr{S}(h_i) = 0$, the value of θ^* for $\sqrt{\frac{\psi^*}{\beta}} = 0$ is $\theta_e = 138°$ ($\frac{h_e}{2R} \simeq 0.872$ and $\frac{\delta_e}{2R} \simeq 1.207$).

Finally, the domain of upwardly travelling slugs may be shared into two regions, progressive slugs (UPS) with $u^* > c^*$ and regressive slugs (URS) with $u^* < c^*$, represented in Fig. 13.

Remembering that $\frac{u^*}{c^*} = \sqrt{\frac{8\sin\theta^*}{\theta^*}\frac{\beta}{\psi^*}}$, u^* is much higher than c^* when $\frac{\psi^*}{\beta}$ is low, provided θ^* be not close to 180°, say for $\theta^* \leqslant 160°$. Then, according to (48) and (56), we have $\omega \simeq U \simeq u^*$, similarly to downward slugs. On the contrary, when $\frac{\psi}{\beta}$ is not low u^* and c^* are generally of the same order of magnitude, with the result that the full relation (48) is to be kept, whereas (56) may be simplified to $U \simeq u^*$ for f^* is close to F. Steady flows corresponding to $u^* = c^*$ belong to this case.

For sufficiently large values of $\frac{\psi^*}{\beta}$, u^* is negligible with regard to c^*, therefore (48) may be approximated by $\omega \simeq -c^*$, U is very low according to (56) and the height h_I defined by $\mathscr{S} = 0$ is necessarily close to h^*. Thereby, regressive slugs are of very small amplitude.

Similarly to downward slugs, information about the amplitude is obtained, but here it originates in the inequality $h_I < h_1$. The value of h_1 must be higher than the lowest possible value of h_I, which fulfills $(\frac{\delta}{\delta^*})^{\frac{1+n}{2-m}} - 1 = \frac{c^*}{\sqrt{2g\delta^*}}\sqrt{\frac{\psi^*}{\beta}}(\frac{a^*}{a} - 1)$ according to (50). Now, at given θ^*, h_I minimum is obtained when $\frac{\psi^*}{\beta} \to 0$. The corresponding solution is $\delta = \delta^*$, which is satisfied by h^*_δ (h^*_δ exists since h^* is larger than $\tilde{h}$). As h^*_δ is a decreasing function of h^*, the smallest value of h^*_δ is obtained when $h^* = H$, yielding $\theta_I = 90°$. Therefore, the minimum of θ_1 is equal to 90° and $\frac{h_1}{2R}$ is necessarily higher than 0.50.

Let us consider for example $\theta^* = 155°$ yielding $\theta_i = 142°$ from Fig. 5. The profile of the interface is drawn in Fig. 14a for three values of $\sqrt{\frac{\psi^*}{\beta}}$. Similarly to Fig. 11a, every curve ends at

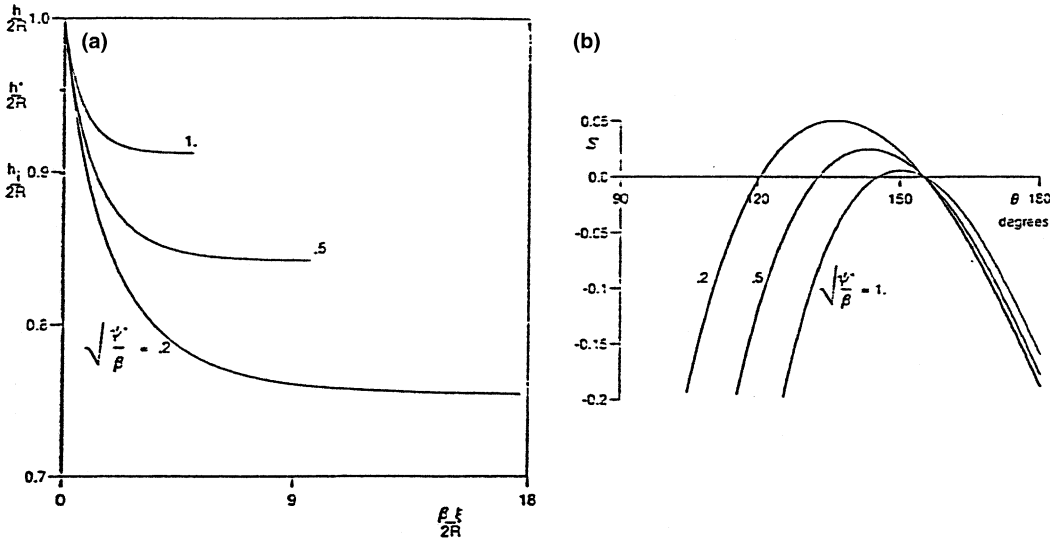

Fig. 14. Upward waves in circular ducts with $\theta^* = 155°$, rough turbulent flow $m = 0$, $n = 1/3$, and three values of $\sqrt{\frac{\psi^*}{\beta}}$: (a) the smooth profile of the interface; (b) the function $\mathscr{S}$.

$h = h_I$. If $\sqrt{\frac{\psi^*}{\beta}} = 0.2$ is chosen, $\theta_I = 121°$ is provided from Fig. 14b, so that in order to construct slugs, θ_1 must lie between 122° and 142°. The longest slug is obtained for $\theta_1 = \theta_I$ ($\frac{h_1}{2R} = 0.765$). Then (15), (48), (56), (27), (43) and (55) provide $u^* = 7.07\sqrt{gR}$, $\omega = 5.16\sqrt{gR}$, $U = 7.04\sqrt{gR}$, $P = 0.335\rho gR$, $\Psi = 1.045\psi^*$ and $\beta L_p = 0.21R$. The length of the bubble is deduced from Fig. 14a with $\beta L_g \simeq 15R$.

8. Validation

8.1. The liquid and gas superficial velocities

For experimental validation, three points will be considered: (i) the transition boundaries and domains of occurrence; (ii) the relation connecting the speed of propagation ω with the velocity U; (iii) the limitation in height of the liquid carpet.

(i) Flow regimes and the transition boundaries are usually plotted using the liquid and gas superficial velocities, $\bar{u}$ and $\bar{v}$ with $A\bar{u}$ and $A\bar{v}$ the liquid and gas volumetric flow rates (Barnea and Taitel, 1986; Taitel and Barnea, 1990).

By definition, $A\bar{u} = \frac{1}{T}\int_0^T au\,dt$ where $T = \frac{L}{\omega}$ is the period of the slug and where the integral is to be computed at constant x. The variable ξ can be used instead of t. For downward slugs, formulae (29) and (30) allow us to write $LA\bar{u} = \int_0^L au\,d\xi = (u^* + c^*)(AL_p + \int_0^{L_g} a\,d\xi) - a^*c^*L$. Finally, thanks to (17), h may take the place of ξ with the result

$$\bar{u} = \frac{u^* + c^*}{L_p + L_g}\left[L_p + \frac{1}{\beta}\int_{h_1}^{H}\left(1 - \frac{a^{*2}c^{*2}}{a^2c^2}\right)\frac{a}{A}\frac{dh}{\mathscr{S}}\right] - \frac{a^*c^*}{A}, \tag{59}$$

L_p, L_g and $\mathscr{S}$ being given by (43), (44) and (31).

The continuity balance for both liquid and gas involves

$$\bar{u} + \bar{v} = U, \tag{60}$$

whence, taking (40) into account,

$$\bar{v} = \frac{u^* + c^*}{L_p + L_g}\left[L_g - \frac{1}{\beta}\int_{h_1}^{H}\left(1 - \frac{a^{*2}c^{*2}}{a^2c^2}\right)\frac{a}{A}\frac{\mathrm{d}h}{\mathscr{S}}\right]. \tag{61}$$

At the transition between roll waves and slugs, we have $h_1 = h_i$ and $L_p = 0$, so the superficial velocities at the onset of slugging are

$$\bar{u}_i = (u^* + c^*)\frac{M_i}{\beta L_i} - \frac{a^*c^*}{A} \tag{62}$$

and

$$\bar{v}_i = (u^* + c^*)\left(1 - \frac{M_i}{\beta L_i}\right), \tag{63}$$

with

$$\beta L_i = \int_{h_i}^{H}\left(1 - \frac{a^{*2}c^{*2}}{a^2c^2}\right)\frac{\mathrm{d}h}{\mathscr{S}} \quad \text{and} \quad M_i = \int_{h_i}^{H}\left(1 - \frac{a^{*2}c^{*2}}{a^2c^2}\right)\frac{a}{A}\frac{\mathrm{d}h}{\mathscr{S}}.$$

Obviously, these velocities can be derived from h^* and $\sqrt{\frac{\psi^*}{\beta}}$ thanks to (15) and (21). Consequently, the domain of downward slug flow of Fig. 10 can be represented in the superficial velocities plane.

Similar results are obtained for upward slugs by changing c^* into $-c^*$ in previous formulae.

The domains of slug flows in circular ducts corresponding to those of Figs. 10 and 13 are plotted in Fig. 15. It appears that the former representation was misleading because downward

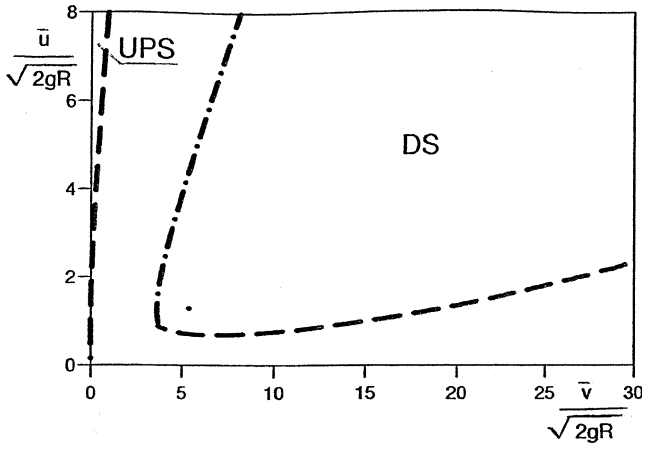

Fig. 15. Domains of slug occurence in circular ducts for rough turbulent flow, $m = 0$, $n = 1/3$. DS: downward slugs; UPS: upward progressive slugs; $---$ $\mathscr{S}(h_i) = 0$; $-\cdot-$ $\mathscr{S}(H) = 0$. The dot represents the example, $\theta^* = 75°$, $\sqrt{\frac{\psi^*}{\beta}} = 0.2$, $\theta_1 = 36°$.

slugs are proved to be the principal ones since they occupy a much larger domain of the velocities plane than upward slugs. In all probability, due to the narrowness of their domain, upward progressive slugs are difficult to detect, and the occurrence of regressive slugs looks most unlikely. The example given in Section 6.3 has been represented in Fig. 15: $\bar{u}/\sqrt{2gR} = 1.29$, $\bar{v}/\sqrt{2gR} = 5.41$ are obtained, yielding $\bar{u} = 0.64$ mm/s, $\bar{v} = 2.68$ mm/s for 2.5 cm in diameter. Relatively low values of the liquid superficial velocity are only obtained in the vicinity of the corner in the DS domain of Fig. 15. Indeed, the actual domain of downward slug occurrence is very small, as already predicted in Section 6.3. This explains why slugs of this kind are so seldom observed.

For given $\bar{u}$ and $\bar{v}$, the three parameters h^*, $\frac{\psi^*}{\beta}$ and h_1 are connected by (59) and (61). Therefore a supplementary datum is necessary for closure. It may be the ratio $\frac{\Psi}{\beta}$ as, according to (41), (60) and (15), we have

$$\frac{\Psi}{\beta} = \left(\frac{\psi^*}{\beta}\right)^{1-\frac{m}{2}} \left(\frac{\delta^*}{\Delta}\right)^{n+\frac{m}{2}} \left(\frac{\sqrt{2g\Delta}}{\bar{u}+\bar{v}}\right)^{m}. \tag{64}$$

Of course, the use of the incoming velocities $\bar{u}$ and $\bar{v}$ and of $\frac{\Psi}{\beta}$ in order to identify a slug flow by means of (59), (61) and (64) seems to have more physical significance than that of h^*, $\frac{\psi^*}{\beta}$ and h_1, because $\bar{u}$, $\bar{v}$ and $\frac{\Psi}{\beta}$ may be prescribed in advance in laboratory experiments. However, once $\bar{u}$ and $\bar{v}$ have been chosen inside the domain of occurrence, the value of $\frac{\Psi}{\beta}$ is to be adjusted in order to satisfy the conditions $h_I < h_1 < h_i$, which cannot be expressed simply with the help of $\bar{u}$, $\bar{v}$ and $\frac{\Psi}{\beta}$.

The maps of progressive slugs, both downward and upward, are superimposed in Fig. 16 on the experimental results by Barnea et al. (1980) for water and air in a duct of 0.025 m in diameter, with a 5° inclination. For this value of R, the comparison between Figs. 10 and 13 and Fig. 3 shows that the whole DS domain and the major part of the UPS domain belong to the region of

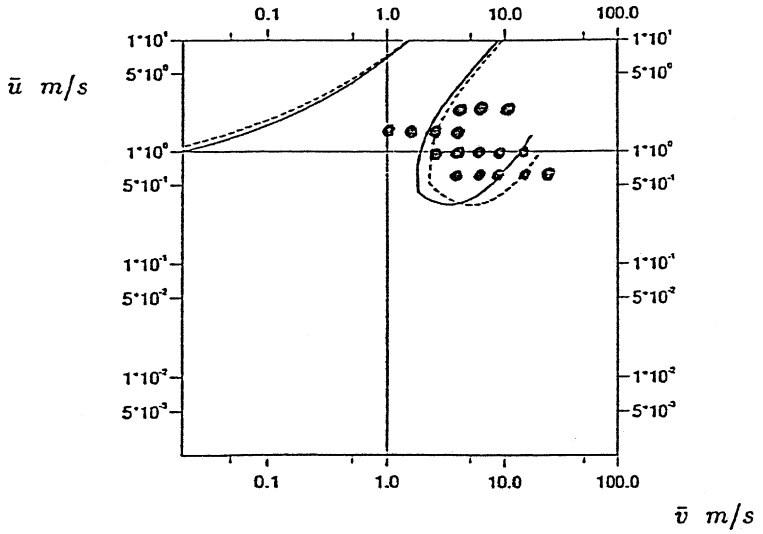

Fig. 16. Comparison with experiments for $R = 1.252 \times 10^{-2}$ m and $\beta = 5°$. Dots represent the experimental data by Barnea et al. (1980). Theoretical onset of slugging, turbulent flow: — $m = 0$, $n = 1/3$; ---- $m = 0$, $n = 0$.

rough turbulent regime. It may be checked that though not accurately predicative, the proposed model of downward slugs provides a satisfactory order of magnitude estimate.

Comparison with other experimental data by Barnea et al. (Barnea et al., 1980, 1982; Barnea and Taitel, 1986) have been made by varying the diameter and the inclination: the agreement remains good, except when the slope is very slight ($\beta \leqslant 1°$), because in this case, the assumption that gravity is dominant is no longer fulfilled.

No slug has been observed by Barnea et al within the upward domain of Fig. 16. Various reasons may be advanced to explain this fact. At first, as previously forecast, this domain may have not been explored owing to its narrowness. Another argument, related to the interfacial stress constitutive law, may be put forward. For upward slugs, u is higher than v as stated in Section 7, so the liquid is now the "driving" medium and then the liquid density should interfere in the interfacial stress instead of the gas density (Brauner and Moalem Maron, 1989), with the consequence that the interfacial stress may become no more negligible (Appendix B).

Nevertheless, upwardly propagating slugs certainly exist as large bubbles with the nose pointing against the flow, according to the sketch of Fig. 12, have been observed (Bendiksen, 1984), a statement which will be born out below.

8.2. The relation between the characteristic velocities

(ii) One of the semi-empirical laws introduced within the frame of the classical approach in order to close the set of equations is the relation between ω and U. Usually

$$\omega = CU + U_{\mathrm{d}} \tag{65}$$

is set where U_{d} is the so-called drift velocity (Taitel and Barnea, 1990).

Various expressions of C and U_{d} have been proposed resulting from dimensional analysis and measurements achieved in circular ducts. Indeed, for downflows, both C and U_{d} are not well-known. The factor C is close to 0.9 in vertical motion and it may exceed 1.2 in almost horizontal ducts, for which some authors claim that U_{d} is negligible.

The comparison of formula (65) with (25) and (26) reveals that in the present theory, $C = 1$ and that U_{d} only depends on the critical state. In fact, C is a velocity profile correction factor (Taitel et al., 2000), so it is not surprising to find $C = 1$ within the frame of one-dimensional theory. Concerning downward slugs, we have seen at the end of Section 6.3 that, being lower than $0.44\sqrt{gR}$ (because of $\theta^* < 90°$), the term Fa^*c^* is negligible, a result consistent with most experimental data.

Conversely, for upward slugs, we have $Fa^*c^* > 1.15\sqrt{gR}$ (because of $\theta^* > 138°$). Corresponding to this case, experiments have shown that ω is lower than U and that U_{d} is negligible (Bendiksen, 1984), a result which agrees with formula (26) and makes the occurrence of upward slugging highly probable.

8.3. The limitation in height

(iii) Regarding the thickness of the liquid layer, an upper limit equal to 0.225 has been found in Section 6 for $\frac{h_1}{2R}$ in case of downward slugging. It is consistent with experiments by Andreussi and Persen (1987), who have observed mean thicknesses of about a quarter of the diameter. This

limitation in height and the fact that L_p is much lower than L_g makes $\bar{v}$ higher than $\bar{u}$ (Figs. 15 and 16).

Concerning upward slugs, h_1 is higher than R as shown in Section 7, a result which cannot be checked due to lack of experimental data.

9. Conclusion

A simple theoretical model of periodic gas–liquid slugs in inclined ducts of arbitrary shape has been worked out. The leading thread of the approach lies in the fact that roll waves and slugs look like linked elements of a common process, the smooth interface being governed in both cases by the same equations and the free bores being replaced by choked bores when the roll waves pattern is replaced by the slug flow one.

The new model presents a universal character, and for this reason it ensures a relative simplicity of application. It does not need any supplementary constitutive law for closure, except the friction law at the wall. The cross-section interferes only by its shape, not by its size, as long as the friction law is valid and as the superficial tension remains negligible.

The case of circular ducts has been investigated and maps of slug occurrence have been displayed. Owing to all the simplifications, no accurate agreement with experiments was expected. Surprisingly, the predicted onset of downward slugging, the most important one, is close to that observed experimentally. Another interesting result is the prediction of upward slugging, which may be related to the "bubble turning" phenomenon (Bendiksen, 1984), a troublesome problem unsolved until the present time (Dukler and Fabre, 1994).

Finally, in spite of strong assumptions, the proposed model turns out to be able to put forward the main properties of periodic slug flows in down sloping ducts with a low pressure gradient along the conduit. It may serve in the future as a guide for further developments. Extension to large inclination may easily be undertaken, with the result that slope and friction will interfere separately, and not only by their ratio. The task is more difficult if slugs in horizontal and upwardly inclined ducts are considered as the effects of gas motion and pressure gradient cannot be neglected for these flows. In this case, owing to the lowness of all friction factors, the gas must move significantly faster than the liquid in order to carry the liquid away against the antagonistic effect of the gravity. Then, the liquid layer is governed by the full equation (B.1) of Appendix B, which is not analytically manageable. Concerning the discontinuities, they still exist, as a definite value of the interface slope is still provided by (B.1), yielding $h(\xi)$ monotonous. As a matter of fact, the analysis is complicated on account of the small gaseous bubbles distributed along the liquid plugs. These dispersed bubbles probably result from the intense melting of both fluids, with zones of reverse flow at the ends of each large bubble, making the assumption of one-dimensional motion highly questionable.

Appendix A

Resulting from (3), we have $k^2 \frac{dk}{dh} \frac{dE}{dh} = 4 \frac{db}{dh} \left(k \frac{dk}{dh} - a \frac{d^2 b}{dh^2}\right) - \frac{kE}{2} \left(\frac{dk}{dh}\right)^2$. The behaviour of δ and E at $h = 0$ and $h = H$ indicates that the equation $E = 0$ has necessarily an odd number of roots, for

which $\frac{dE}{dh}$ and $\frac{db}{dh}$ have the same sign. As b cancels at the bottom and at the top, the assumption $\frac{d^2b}{dh^2} < 0$ means that b has only one maximum, say b_W at $h = h_W$ where E is positive, as $a < bk$, and $\frac{dE}{dh}$ negative. For the lowest root of $E = 0$, say $\tilde{h}$, $\frac{dE}{dh}$ is positive if $\frac{db}{dh} > 0$, which is impossible as that requires another root, lower than $\tilde{h}$: then $\frac{db}{dh} < 0$ is necessary, with the result $\tilde{h} > h_W$. Moreover, as $E = 0$ and $\frac{dE}{dh} > 0$ cannot be achieved for $h > h_W$, no root higher than $\tilde{h}$ exists. Consequently, $\tilde{h}$ the only root.

Thus finally, $\frac{dE}{dh}$ is always negative, so that δ is a concave function with one maximum.

Appendix B

Thanks to $u = \omega - \frac{q}{a}$ and $v = \omega$, the momentum equations for the liquid and the gas are

$$\left(1 - \frac{q^2 b}{ga^3}\right) g \frac{dh}{d\xi} - g\beta + \frac{1}{\rho}\frac{d\bar{p}}{d\xi} + \frac{\psi u^2}{2\delta} - \frac{\varepsilon\bar{\psi} q^2 b}{2a^3} = 0$$

and

$$\frac{1}{\rho}\frac{d\bar{p}}{d\xi} + \frac{\chi\psi'\omega^2(K-k)}{8(A-a)} + \frac{\varepsilon\bar{\psi} q^2 b}{2a^2(A-a)} = 0,$$

where $\chi\rho$ is the gas density, $\bar{p}$ the pressure at the interface (equal to the gas pressure), ψ' the gas friction factor at the wall and $\bar{\psi}$ the friction factor at the interface. According to Brauner and Moalem Maron (1989), $\varepsilon = \chi$ when $\omega > u$ and $\varepsilon = -1$ when $\omega < u$.

The elimination of $\bar{p}$ leads to

$$\left(1 - \frac{q^2 b}{ga^3}\right)\frac{dh}{d\xi} - \beta + \frac{\psi u^2}{2g\delta} - \frac{\chi\psi'\omega^2(K-k)}{8g(A-a)} - \frac{\varepsilon\bar{\psi} q^2 Ab}{2ga^3(A-a)} = 0. \tag{B.1}$$

Let us take into account $\chi \ll 1$ and consider that all friction factors are of the same order of magnitude. We suppose that the liquid velocity satisfies

$$u \gg \chi^{1/2}\omega,$$

which is met in particular when $u \sim \omega$, i.e. $u \sim v$.

If $\omega > u$, the two last terms in Eq. (B.1) are negligible and Eq. (14) is recovered. On the contrary, if $\omega < u$ the last term in (B.1) is to be kept, except when u is close to ω, making both q and $\bar{\psi}$ very low.

References

Andreussi, P., Persen, L.N., 1987. Stratified gas–liquid flow in downwardly inclined pipes. Int. J. Multiphase Flow 13, 565–575.

Barnea, D., Shoham, O., Taitel, Y., 1982. Flow pattern transition for downward inclined two phase flow: horizontal to vertical. Chem. Eng. Sci. 37 (5), 735–740.

Barnea, D., Shoham, O., Taitel, Y., Dukler, A., 1980. Flow pattern transition for gas–liquid flow in horizontal and inclined pipes. Int. J. Multiphase Flow 6, 217–225.

Barnea, D., Taitel, Y., 1986. Flow pattern transition in two phase gas–liquid flows. Encyclopedia Fl. Mech. Ed. Cheremissinoff, Gulf. Pub. 3, 403–474.

Bendiksen, K.H., 1984. An experimental investigation of the motion of long bubbles in inclined tubes. Int. J. Multiphase Flow 10, 467–483.

Boudlal, A., Dyment, A., 1996. Weakly nonlinear interfacial waves in a duct of arbitrary cross-section. Eur. J. Mech. B/Fluids 15 (3), 331–366.

Brauner, N., Moalem Maron, D., 1989. Moalem flow phase liquid–liquid stratified flow. Physico-chem. Hydrodyn. 11, 487–506.

Dressler, R.F., 1949. Mathematical solution of the problem of roll-waves in inclined open channels. Comm. Pure. Appl. Math. 2, 149–194.

Dukler, A., Fabre, J., 1994. Gas liquid slug flow: knots and loose ends. In: Two Phase Fundamentals, vol. 8. Hewitt G.F. Begell House, pp. 355–470.

Dukler, A., Hubbard, M., 1975. A model for gas–liquid slug flow in horizontal and near horizontal tubes. Ind. Eng. Chem. Fundam. 14, 337–347.

Dyment, A., 1981. Phenomènes exceptionnels de propagation d'ondes de pesanteur dans un canal. J. de Mécanique 2, 59–78.

Dyment, A., 1998. Finite amplitude hydraulic jumps in partly filled conduits of arbitrary shape. C. R. Acad. Sci. 326 (IIb), 179–184.

Fan, Z., Ruder, Z., Hanratty, T., 1993. Pressure profiles for slugs in horizontal pipe lines. Int. J. Multiphase Flow 19 (3), 421–437.

Kranenburg, C., 1992. On the evolution of roll waves. J. Fl. Mech. 245, 249–261.

Liapidevskii, V.Y., 2000. The structure of roll waves in two layer flows. J. Appl. Math. Mech. 64 (6), 937–943.

Lin, P.Y., Hanratty, T., 1986. Prediction of the initiation of slugs with linear stability theory. Int. J. Multiphase Flow 12 (3), 79–98.

Taitel, Y., Barnea, D., 1990. Two phase slug flow. Adv. Heat Transfer 20, 83–132.

Taitel, Y., Dukler, A., 1976. A model for predicting flow regime transition in horizontal and near horizontal gas–liquid flow. AIChE. J. 22, 47–55.

Taitel, Y., Sarica, C., Brill, J., 2000. Slug flow modelling for downward inclined pipe flow: theoretical consideration. Int. J. Multiphase Flow 26, 833–844.

Whitham, G.B., 1974. Linear and Nonlinear Waves. Wiley.

Woods, B., Hurlburt, E.T., Hanratty, T.J., 2000. Mechanism of slug formation in downwardly inclined pipes. Int. J. Multiphase Flow 26, 977–998.

Yu, J., Kevorkian, J., 1992. Nonlinear evolution of small disturbances into roll waves in an inclined open channel. J. Fl. Mech. 243, 575–594.